



## Ice-Nucleating Particles Near Two Major Dust Source Regions

Charlotte M. Beall<sup>1,2</sup>, Thomas C. J. Hill<sup>3</sup>, Paul J. DeMott<sup>3</sup>, Tobias Köneman<sup>2\*</sup>, Michael Pikridas<sup>4</sup>,  
Frank Drewnick<sup>5</sup>, Hartwig Harder<sup>6</sup>, Christopher Pöhlker<sup>2</sup>, Jos Lelieveld<sup>4,6</sup>, Bettina Weber<sup>2\*\*</sup>,  
Minas Iakovides<sup>4</sup>, Roman Prokeš<sup>7,8</sup>, Jean Sciare<sup>4</sup>, Meinrat O. Andreae<sup>1,2,9</sup>, M. Dale Stokes<sup>1</sup>,  
Kimberly A. Prather<sup>1,10</sup>

<sup>1</sup>Scripps Institution of Oceanography, University of California San Diego, La Jolla, CA 92037, USA

<sup>2</sup>Max Planck Institute for Chemistry, Multiphase Chemistry and Biogeochemistry Departments, D-55128 Mainz, Germany

<sup>3</sup>Department of Atmospheric Science, Colorado State University, Fort Collins, CO 80523, USA

<sup>4</sup>Climate & Atmosphere Research Center, The Cyprus Institute, Nicosia, CY-1645, Cyprus

<sup>5</sup>Max Planck Institute for Chemistry, Particle Chemistry Department, D-55128 Mainz, Germany

<sup>6</sup>Max Planck Institute for Chemistry, Atmospheric Chemistry Department, D-55128 Mainz, Germany

<sup>7</sup>RECETOX, Faculty of Science, Masaryk University, Kotlarska 2, 611 Brno, Czech Republic

<sup>8</sup>Department of Atmospheric Matter Fluxes and Long-range Transport, Global Change Research Institute of the Czech Academy of Sciences, Belidla 4a, 60300, Brno, Czech Republic

<sup>9</sup>Department of Geology and Geophysics, King Saud University, Riyadh, Saudi Arabia

<sup>10</sup>Department of Chemistry and Biochemistry, University of California San Diego, La Jolla, CA, 92093 USA

\*Now at Envicontrol GmbH, Waidmarkt 11, 50676 Köln, Germany

\*\*Now at: Institute of Biology, University of Graz, 8010 Graz, Austria



32 Correspondence to: Charlotte M. Beall, [cbeall@ucsd.edu](mailto:cbeall@ucsd.edu)

### 33 Abstract

34 Mineral dust and sea spray aerosol represent important sources of ice nucleating particles (INPs), the minor  
35 fraction of aerosol particles able to trigger cloud ice crystal formation and, consequently, influence multiple  
36 climate-relevant cloud properties including lifetime, reflectivity, and precipitation efficiency. Mineral dust  
37 is considered the dominant INP source in many parts of the world due to its ice nucleation efficiency and  
38 its sheer abundance, with global emission rates of up to 4700 Tg a<sup>-1</sup>. However, INPs emitted from the ocean  
39 surface in sea spray aerosol frequently dominate INP populations in remote marine environments, including  
40 parts of the Southern Ocean where cloud-resolving model simulations have demonstrated that cloud  
41 reflectivity is likely strongly controlled by INPs. Here we report INP concentrations measured in aerosol  
42 and seawater samples during Air Quality and Climate Change in the Arabian BASin (AQABA), a shipborne  
43 campaign that spanned the Red Sea, Gulf of Aden, Arabian Sea, Arabian Gulf, and part of the  
44 Mediterranean. In aerosol samples collected within a few hundred kilometers of the first and second ranked  
45 sources of dust globally, the Sahara and Arabian Peninsula, INP concentrations ranged from 0.2 to 11 L<sup>-1</sup>  
46 at -20 °C with observed ice nucleation site densities ( $n_s$ ) 1-3 orders of magnitude below levels predicted by  
47 mineral dust INP parameterizations. Over half of the samples (at least 14 of 26) were collected during dust  
48 storms with average dust mass concentrations between 150 and 490 µg m<sup>-3</sup> (PM<sub>10</sub>). The impacts of heat and  
49 peroxide treatments indicate that organics were responsible for the observed ice nucleation (IN) -activity at  
50 temperatures ≥ -15 °C with proteinaceous (heat-labile) INPs frequently observed at higher freezing  
51 temperatures > -10 °C. Overall, results demonstrate that despite proximity to the Sahara and the Arabian  
52 Peninsula and the dominance of mineral dust in the aerosol sampled, existing mineral dust  
53 parameterizations alone would not skillfully represent the near-surface  $n_s$  in the observed temperature  
54 regime (-6 to -25 °C). The decreased  $n_s$ , and results demonstrating that organics dominated the observed  
55 IN activity > -15 °C, indicate that the IN-active organic species are limited compared to the mineral IN  
56 components of dust. Future efforts to develop or improve representations of dust INPs at modest  
57 supercooling (> -15 °C) would benefit from a characterization of the specific organic species associated  
58 with dust INPs. More generally, an improved understanding of the organic species associated with  
59 increased IN -activity and their variability across dust source regions would directly inform efforts to  
60 determine whether  $n_s$ -based parameterizations are appropriate for faithful representation of dust INPs in  
61 this sensitive temperature regime, whether region-specific parameterizations are required, or whether an  
62 alternative to the  $n_s$  approach is necessary.



## 63 1 Introduction

64 Ice-nucleating particles (INPs) modulate the temperature and relative humidity at which ice  
65 particle formation occurs in the atmosphere and thus are a key factor that controls ice-phase  
66 partitioning in clouds. As initiators of ice formation and related phase-partitioning processes, INPs  
67 affect multiple cloud properties and exert a strong influence on cloud lifetime, reflectivity and  
68 precipitation efficiency (e.g. Lohmann and Feichter, 2005; Vergara-Temprado et al., 2018).

69 Globally, desert dust is likely the most abundant aerosol type by mass (Kinne et al., 2006; Kok et  
70 al., 2021). Furthermore, multiple studies have demonstrated that mineral dust is the dominant ice-  
71 nucleating (IN) species in many parts of the world based on observations (Ardon-Dryer and Levin,  
72 2014; Boose et al., 2016; DeMott et al., 2015a; Price et al., 2018) and modeling of global INP  
73 distributions (Burrows et al., 2013; Hoose et al., 2010; Murray et al., 2012; Vergara-Temprado et  
74 al., 2017). Annual global dust emission rate estimates range between 400 and 4700 Tg a<sup>-1</sup> (Huneeus  
75 et al., 2011; Kok et al., 2021). Of the global dust loading in the atmosphere (20-29 Tg), North  
76 African source regions are estimated to contribute ~50% (11-15 Tg), and the Middle East and  
77 Central Asian source regions account for the bulk of the remainder, ~30% (7.7 Tg) (Kok et al.,  
78 2021). Analysis of satellite products indicates that dust emissions rates are increasing over the  
79 Middle East at a rate of 15% a<sup>-1</sup> (Klingmüller et al., 2016; Yu et al., 2018).

80 While Hoose and Möhler (2012) showed that mineral dust INPs generally activate ice crystals at  
81 freezing temperatures < -15 °C, dust containing K-feldspar has been shown to nucleate ice at much  
82 warmer temperatures, up to -4 °C (Atkinson et al., 2013; Harrison et al., 2016; Niedermeier et al.,  
83 2015; Wex et al., 2014; Whale et al., 2015; Zolles et al., 2015). K-feldspars represent up to ~24%  
84 of Saharan and Asian dusts by mass (Nickovic et al., 2012). However, knowledge of the abundance  
85 and the available surface fraction of aerosolized K-feldspar would be necessary to evaluate the IN  
86 efficiency of dust at temperatures > -15 °C (Kanji et al., 2017).

87 Though mineral dust is considered to be the dominant INP source in many regions, multiple  
88 modeling and observational studies suggest that marine INPs are frequently dominant in remote  
89 ocean regions in air masses with low concentrations of terrestrial aerosol (McCluskey et al., 2018b,  
90 2018c; Vergara-Temprado et al., 2017; Wilson et al., 2015; DeMott et al., 2016). Using a global  
91 aerosol model to simulate marine organic and K-feldspar INP populations, Vergara-Temprado et



92 al. (2017) showed that the relative contribution of marine organic vs. dust INPs in remote regions  
93 varies seasonally, and that marine organic INPs frequently outnumber K-feldspar INPs (up to  
94 100% of the simulated days in the Southern Ocean during summer). Results from a follow-on  
95 cloud-resolving model study showed that Southern Ocean cloud reflectivity is strongly modulated  
96 by INP concentrations, indicating that accurate estimates of the radiative energy budget in the  
97 Southern Ocean likely require improved and reliable representation of both dust and marine  
98 organic INPs (Vergara-Temprado et al., 2018). By generating isolated nascent sea spray aerosol  
99 over a range of biological conditions, mesocosm studies have shown that marine INPs are  
100 comprised of two classes: a dissolved organic carbon (DOC) type composed of IN-active  
101 molecules and a particulate organic carbon (POC) type linked to the death phase of phytoplankton  
102 blooms (McCluskey et al., 2017, 2018a).

103 Parameterizations for both marine and mineral dust populations are commonly implemented in  
104 atmospheric models to estimate dust and marine INP concentrations. There are multiple existing  
105 mineral dust INP parameterizations used to estimate their concentrations in aerosolized desert dust,  
106 some based exclusively on laboratory measurements (e.g., Niemand et al., 2012; Ullrich et al.,  
107 2017), and others derived from a combination of laboratory and field measurements (DeMott et  
108 al., 2015). There are, additionally, multiple mineral-specific INP parameterizations including illite  
109 (Broadley et al., 2012), kaolinite (Welti et al., 2012), quartz (Harrison et al., 2019) and K-feldspar  
110 (Atkinson et al., 2013). The parameterizations by Ullrich et al. (2017, hereafter, “U17”) and  
111 Niemand et al. (2012, “N12”) were developed using dust samples from multiple deserts, and both  
112 found little variability in the IN activity between dusts from locations as disparate as the Sahara  
113 and Asia. DeMott et al. (2015, “D15”) found agreement between their observations-based  
114 parameterization and N12, supporting the validity of laboratory-based parameterizations. Results  
115 in D15 also confirmed the conclusions of N12 and U17: that to first order, dusts from distinct  
116 regions can be parameterized as a single particle type. The D15 parameterization has been  
117 considered to be representative of dust that has undergone atmospheric photochemical and  
118 oxidative processes in transport (i.e., “aged” dust), because the parameterization was derived from  
119 observations made far (1000s of kilometers) from the dust emissions sources (Boose et al., 2016).

120 By contrast, few studies report INP measurements near (e.g., < 1 day of transport) a major dust  
121 source, and the lack of observations near dust source regions inhibit the evaluation of the ability



of existing dust INP parameterizations to represent nascent dust populations (Boose et al., 2016; Gong et al., 2020; Price et al., 2018). INP observations are particularly lacking for the sensitive temperature regime  $> -20$  °C. Boose et al. (2016) found that D15 overpredicted INPs observed during Saharan dust events at a location within 100s of km of the Sahara (Izaña, Tenerife, Spain) by 2-3 orders of magnitude, suggesting that aging may lead to increased IN efficiency in mineral dust and that D15 may be less representative of nascent dust. These conclusions were supported by Conen et al. (2015), who found that concentrations of INPs at  $-20$  °C measured during Saharan dust events were one order of magnitude higher at Jungfraujoch in the Swiss Alps than in Izaña, where dust events had occurred 1-7 d prior to reaching Jungfraujoch. Gong et al. (2020) measured INPs in a variety of atmospheric and seawater sample types at Cabo Verde and determined mineral dust to be the dominant source of INPs observed in the atmosphere but found that INPs with freezing temperatures  $> -10$  °C were likely biological. At altitudes between 30 and 3500 m in the same region, Price et al. (2018) found that measured concentrations of INPs ranged two orders of magnitude at a given temperature, and that the observed concentrations related to the atmospheric dust loadings.

Recently, multiple studies have provided new, much-needed observations of ambient atmospheric INPs in marine environments (DeMott et al., 2016; Hartmann et al., 2020; McCluskey et al., 2018b, 2018c; Yang et al., 2020) where data was historically lacking and, consequently, an impediment to achieving predictive understanding of global INP distributions (Burrows et al., 2013). There are now two parameterizations available for the estimation of atmospheric concentrations of marine INPs emitted from the ocean surface: Wilson et al. (2015), which estimates cumulative INPs from total organic carbon (TOC) concentrations in simulated SSA, and McCluskey et al. (2018), which estimates ice nucleation site density ( $n_s$ ) from aerosol surface area. Wilson et al. (2015) and McCluskey et al. (2018) derived marine INP parameterizations from field measurements of INPs in Atlantic and Arctic Ocean sea surface microlayer samples and pristine SSA samples over the North Atlantic Ocean, respectively.

Here, we report observations of INPs measured in air masses influenced by both desert dust and marine aerosol (Edtbauer et al., 2020) in close proximity to the two greatest global dust aerosol sources: the Sahara (#1) and the Arabian Peninsula (#2) (Kok et al., 2021). INP concentrations were measured in 26 aerosol samples collected during Air Quality and Climate Change in the



152 Arabian BASin (AQABA), a shipborne campaign which took place July – August 2017 on a  
153 transect that spanned the central and eastern parts of the Mediterranean, the Red Sea, the Gulf of  
154 Aden, the Arabian Sea and Arabian Gulf. Observed  $n_s$  were compared to dust and marine INP  
155 parameterizations, and the contributions of heat-labile (e.g., proteinaceous) and organic  
156 compounds to observed INP populations were assessed via heat and peroxide treatments. Finally,  
157 the potential INP source strengths of subsurface seawater (SSW) were assessed and compared with  
158 SSW INP measurements from prior studies of remote and coastal seawater.

## 159 2 Methods

### 160 2.1 Project Overview

161 The AQABA campaign was conducted from 25 June to 3 September 2017 onboard the RV  
162 *Kommandor Iona*. The research voyage was conducted in two transects: the first leg beginning in  
163 La-Seyne-sur-Mer, France, heading through the Suez Canal, around the Arabian Peninsula and  
164 ending in Kuwait, and second leg a return transect via the same route (Fig. S1-S2). The campaign  
165 supported a large suite of on- and offline aerosol and gas-phase measurements (Bourtsoukidis et  
166 al., 2019, 2020; Celik et al., 2020; Edtbauer et al., 2020; Eger et al., 2019; Friedrich et al., 2021;  
167 Pfannerstill et al., 2019; Tadic et al., 2020; Wang et al., 2020).

### 168 2.2 Aerosol and Trace Gas Measurements

169 Aerosol size distributions were measured using an Optical Particle Spectrometer (OPC, Grimm  
170 model 1.109) and a Fast Mobility Particle Spectrometer (FMPS, TSI model 3091). The OPC  
171 measures particles in the size range 0.25 – 32  $\mu\text{m}$ , and the FMPS measures particles with sizes  
172 between 5.6 nm and 560 nm. The inlet for the aerosol instrumentation was located at the top of a  
173 measurement container at a distance of about 25 m from the INP filter sampling unit. To avoid  
174 condensation in inlet lines, aerosol samples were passed through a drying system, which reduced  
175 ambient relative humidity to an average value of  $\approx 40\%$  in the measurement container. Two  
176 additional measurements provided aerosol data from which a filter flag intended to identify and  
177 eliminate stack emissions was derived: particle number concentrations as measured by a  
178 Condensation Particle Counter (CPC, TSI model 3787) and black carbon concentrations  
179 (Aethalometer, Magee AE33). The filter flag, based on short term variation in particle number



180 concentration, black carbon concentration, wind direction and speed, was applied to all aerosol  
181 data so that samples contaminated by stack emissions could be identified.

182 Particle surface area concentrations were derived from FMPS and OPC measurements as follows.  
183 Geometric diameters were estimated from the measured mobility diameters (FMPS) and optical  
184 particle diameters (OPC). Aerosols were assumed dry at sampling conditions following the drying  
185 system described above. To convert optical particle diameters into geometric diameters, it was  
186 assumed that all coarse particles ( $d_p > 3000$  nm) were composed of sea salt and dust with a mass  
187 ratio of 25% to 75%, and for the respective refractive indices and shapes the measured optical  
188 particle diameters were converted into geometric diameters. Fine particle ( $d_p < 700$  nm) sizes were  
189 converted from  $d_{opt}$  into  $d_{geo}$  using the optical properties calculated from the  $PM_{10}$  chemical  
190 composition as measured by an Aerosol Mass Spectrometer (Aerodyne HR-ToF-AMS), assuming  
191 spherical particles. For particles in the intermediate size range (700 – 3000 nm), log-linear  
192 interpolation of optical and spherical properties was applied for conversion of optical into  
193 geometric particle diameters. The mobility diameters measured by the FMPS were considered  
194 equivalent to the geometric diameter, assuming spherical particles. From the resulting particle size  
195 distributions, particle surface area was calculated for each size bin. Total particle surface  
196 concentrations were determined by integrating the surface area distribution for particles up to 10  
197  $\mu m$ . The overall uncertainty of derived particle surface area concentrations is estimated to be 30%.

198 The water-soluble fraction of total suspended particles (TSPs) was monitored with hourly  
199 resolution using a Monitor for AeRosols and Gases in Ambient Air, MARGA (Metrohm Applikon  
200 model S2, Herisau, Switzerland). Sea salt concentrations were estimated by scaling measured  
201 soluble  $Na^+$  concentrations by 3.27 following Manders et al. (2009). Hourly composition data was  
202 linearly interpolated for 4 samples where 1-3 hours (of 7-24 hours total sampling time) was missing  
203 (Fig. S3).

204 Nitric oxide (NO) concentrations were measured using a commercially available two-channel  
205 chemiluminescence monitor, CLD 790 SR (ECO Physics AG, Dürnten, Switzerland). During the  
206 AQABA campaign, the CLD 790 SR, MARGA, FMPS, OPC, HR-ToF-AMS, CPC and





207 Aethalometer were operated within laboratory containers on the main deck of the research vessel.  
208 The NO measurements were used to prevent stack sampling during INP collection (see Sect. 2.4).

### 209 **2.3 Dust Mass Concentrations from MERRA**

210 Area-averaged hourly dust surface mass concentrations along the cruise track were obtained from  
211 the (0.5 x 0.625 °) Modern-Era Retrospective analysis for Research and Application, version 2  
212 (MERRA-2; Gelaro et al., 2017). MERRA-2 uses the GEOS-5 Earth system model (Molod et al.,  
213 2015; Rienecker et al., 2011) with 72 vertical layers between the surface and 0.01 hPa (~ 80 km)  
214 and the three-dimensional variational data assimilation Gridpoint Statistical Interpolation analysis  
215 system (Kleist et al., 2009; Wu et al., 2002). It simulates 5 types of aerosols (dust, sea salt, sulfate  
216 and black and organic carbon) using the Goddard Chemistry, Aerosol, Radiation, and Transport  
217 (GOCART) model (Chin et al., 2002; Colarco et al., 2010). Dust emissions and deposition rates in  
218 MERRA-2 are estimated by summing the emissions and deposition rates across GOCART  
219 simulated dust particles between 0.1 - 10 µm in size (dry diameter) (Gelaro et al., 2017). Dust  
220 emissions are constrained by wind-driven erosion over the source locations, which are identified  
221 from the topographic depression map (Ginoux et al., 2001). Aerosol observations are derived from  
222 various satellite products and are jointly assimilated within GEOS-5 with meteorological  
223 observations (Buchard et al., 2017). MERRA-2 has been shown to successfully reproduce the  
224 interannual variability of North-Atlantic dust transport. Additionally, the improved aerosol  
225 assimilation scheme in MERRA-2 was shown to have a positive impact on the representation of  
226 long-range dust transport from the Sahara compared to prior versions (Buchard et al., 2017).

### 227 **2.4 Measurement of Ice Nucleating Particles**

228 Ambient aerosol sampling for offline measurement of INPs was conducted from 5 Jul – 31 Aug  
229 2017 on the *Kommandor Iona's* wheelhouse top (platform above the bridge), ~25 m from the  
230 online aerosol measurements inlet and ~35 m from the ocean surface (Fig. S4). Sampling locations  
231 along the cruise transect corresponding to each aerosol sample are shown in Figs. S1-2.

232 Aerosol samples were collected over 3-28 hour periods on polycarbonate filters (47 mm diameter,  
233 0.2 µm pore-size, Whatman® Nuclepore, Chicago, Illinois, USA) placed in open-face Nalgene®  
234 Analytical Filter Units (Waltham, Massachusetts, USA). Aerosol sampling flow rates through the





filter units were set to 10-13 Lpm using a MassStream<sup>TM</sup> mass flow controller (Bethlehem, PA, USA) connected inline with a rotary vane pump (Thomas QR-0100, Gardner Denver ©, Monroe, LA, USA). To decrease exposure to stack emissions, the pump was automated to switch off when online measurements of NO exceeded one standard deviation above the average background concentration for over 1 minute ( $\sim 0.4 \pm 0.8$  ppb). Comparing the stack contamination filter flag for aerosol measurements (Sec. 2.2) with INP sampling periods additionally indicates no influence of stack emissions on INP filter samples.

Prior to sampling, filters were cleaned by soaking in 10 % H<sub>2</sub>O<sub>2</sub> for 10 minutes followed by rinsing three times with deionized water, the last rinse further “polished” by passage through a 0.1  $\mu$ m pore-size syringe filter (Puradisc, Whatman®, Maidstone, U.K). Filters were pre-loaded into filter units in a laminar flow hood to further minimize contamination from handling. After collection, each aerosol filter was placed in a 60 mm diameter sterile Petri dish (Life Science Products, Frederick, Colorado, USA) using pre-cleaned acetyl plastic forceps (Fine Science Tools, Foster City, California, USA), sealed with Parafilm and stored frozen (-20 °C). Samples were shipped in a dry shipper via Cryoport® High Vol Shipper at -180 °C and upon arrival at the laboratory were stored at -80 °C until processed, within 18 to 38 months of collection. To release collected particles, filters were immersed in 5-8 mL ultrapure water (Cat. Number W4502, Sigma-Aldrich®, St. Louis, MO, USA) and shaken for 20 minutes just prior to measurement. Eight samples were additionally diluted 100-fold to measure INP concentrations at lower freezing temperatures (Fig. S5).

INP concentrations were measured using the SIO-Automated Ice Spectrometer (SIO-AIS), an immersion freezing droplet assay instrument that is described in detail in Beall et al. (2017). Briefly, the aerosol sample suspensions and SSW samples were distributed in 30 x 50- $\mu$ L aliquots into clean 96-well polypropylene sample trays (OPTIMUM® ULTRA Brand, Life Science Products). An equal number and volume of aliquots of ultrapure water accompanied each sample in the tray as a control. Trays were then inserted into an aluminum block that was cooled at -0.87 °C min<sup>-1</sup> until the samples are frozen. Cumulative INP number concentrations per temperature per volume liquid are calculated using the fraction (*f*) of unfrozen wells per given temperature interval:



$$n_{INP,L} = \frac{-\ln(f)}{V_d} \quad \text{Eq. (1)}$$

265

266 where  $V_d$  is the volume of the sample in each well. For aerosol filter samples, cumulative INP  
 267 number concentrations are calculated using the ratio of the volume used for resuspension of the  
 268 particles ( $V_{re}$ ) to the volume of air sampled ( $V_A$ ):

269

$$n_{INP} = \frac{-\ln(f) \cdot V_{re}}{V_d \cdot V_A} \quad \text{Eq. (2)}$$

271

272 Prior to calculating  $n_{INP}$ , the fraction of unfrozen wells ( $f$ ) was adjusted for contamination in the  
 273 water used for suspension by subtracting the number of frozen ultrapure water wells per  
 274 temperature interval from both the total number of unfrozen wells and total wells of the sample.  
 275 The  $n_{INP}$  was additionally adjusted for background INPs from filters and sampling handling  
 276 processes. Background INP concentrations were estimated using measured INP concentrations in  
 277 aerosol sample field blanks, which had been momentarily placed in the sampling apparatus before  
 278 removal and unloading and storage of the filter. Seven field blank samples were collected, one  
 279 every ~ 7 days of the cruise (Fig. S6). INP concentrations were measured in field blanks as  
 280 described above, and the  $n_{INP}$  simulated using the mean air volume sampled (6680 L). Figure S6  
 281 shows the estimated  $n_{INP}$  across the 7 field blanks, which ranged between  $3.0 \times 10^{-4}$  and  $3.0 \times 10^{-}$   
 282  $^2 \text{ L}^{-1}$  at  $-20^\circ \text{C}$ . The freezing onset temperatures detected in the field blanks ranged between  $-6$  and  
 283  $-27^\circ \text{C}$ . To correct  $n_{INP}$  measured in aerosol samples for background INPs from sample handling,  
 284 a linear regression of the average INP concentration measured in field blank suspensions ( $\text{mL}^{-1}$   
 285 water) was used to estimate background concentrations of INPs in samples at all temperatures  
 286 between  $-14.5^\circ \text{C}$  and  $-27^\circ \text{C}$ . The estimated background INP concentration was then subtracted  
 287 from the INP concentration measured in filter sample suspension volumes in this temperature  
 288 range prior to calculating  $n_{INP}$ . The  $n_{INP}$  measured in one aerosol sample (f033) fell within the  
 289 estimated INP background levels.

290 For this study, the detection limit was  $0.68 \text{ INPs mL}^{-1}$  liquid or  $0.001\text{-}0.0024 \text{ INPs L}^{-1}$  air for the  
 291 maximum and minimum air volume sampled, respectively. To extend the upper limit of detection



(i.e., the point at which all droplets have frozen) dilutions of 1:10 and 1:100 were performed on 8 samples (Fig. S5).

The ice-active surface site density,  $n_s$ , is a metric used to define the ice-nucleating capabilities of an aerosol species (i.e., an aerosol sample of all the same particle type) (Kanjilal et al., 2017) as follows:

$$n_s = \frac{N_{ice}}{N_{tot} \times A \text{ (cm}^2\text{)}} \quad \text{Eq. (3)}$$

where  $N_{ice}$  is the number of frozen droplets,  $N_{tot}$  is the total number of particles in a monodisperse aerosol population, and  $A$  is the surface area per particle.

The value of  $n_s$  can also be approximated for polydisperse aerosol samples containing multiple aerosol types:

$$n_s = \frac{N_{ice}}{A_{tot} \text{ (cm}^2\text{)}} \quad \text{Eq. (4)}$$

where  $A_{tot}$  is the total surface area of the polydisperse aerosol sample. The difference between the  $n_s$  approximation (Eq. 4) and  $n_s$  (Eq. 3) is that many particle types are typically included in the  $n_s$  approximation, and in an ambient aerosol measurement most of these are not ice nucleating. Furthermore, the subset of INPs in the sample are likely also of different types, which likely have different  $n_s$  in the strict sense (Eq. 3). Nevertheless, the  $n_s$  approximation is a useful metric for comparing the ice-nucleating ability of different air masses and source regions and is often used for comparing data across studies of INPs measured in ambient air. It is extremely challenging to separate measurements of INPs and surface area by each particle type, and requires, for example, combining online measurements of single particle chemistry, size distributions and INPs (Cornwell et al., 2019). All  $n_{INP}$  and  $n_s$  are reported normalized to a standard temperature of 273.15 °K and pressure of 1013 hPa.

Heat and hydrogen peroxide treatments were applied to a subset of samples (12 of 26) to test for heat-labile biological (e.g., proteinaceous) and organic INP composition, respectively (McCluskey et al., 2018b; Suski et al., 2018). For each heat-treated sample, a 2 mL aliquot of the original ultrapure water suspension was heated to 95 °C for 20 min in a water bath and re-tested to assess the reduction in INP concentrations. For peroxide treatments, 1.6 mL of the original suspension was combined with 0.8 mL of 30%  $\text{H}_2\text{O}_2$  (Sigma Aldrich®, St. Louis, Missouri, USA) to achieve



320 a final concentration of 10%, then the mixture was immersed in water, and heated to 95 °C for 20  
321 min while being illuminated with two 26-W UVB fluorescent bulbs to generate hydroxyl radicals.  
322 To remove residual H<sub>2</sub>O<sub>2</sub>, to prevent otherwise significant freezing point depression, the solution  
323 was cooled and catalase (Cat. number IC10042910, MP Biomedicals, Santa Ana, California, USA)  
324 was added. Since catalase is itself decomposed by H<sub>2</sub>O<sub>2</sub>, while simultaneously catalyzing  
325 peroxide's disproportionation into water and oxygen, the enzyme was added in several 20 µL  
326 aliquots, allowing several minutes between each, until no effervescence resulted upon its addition.  
327 Fisher's Exact Test was applied to frozen and unfrozen well fractions between each untreated  
328 sample and its corresponding treated sample to test for significant differences ( $p < 0.05$ ). Note  
329 that significant difference in frozen well fraction is insufficient as a sole indicator of sensitivity in  
330 peroxide treated samples because samples are diluted 2:3 (by 33%) compared to untreated samples.  
331 As INP concentrations can be corrected for the dilution by scaling (as opposed to frozen well  
332 fractions), the overlap in 95% binomial sampling confidence intervals (Agresti and Coull, 1998)  
333 between the untreated and peroxide-treated sample is an additional indicator of sensitivity for a  
334 given data point in the peroxide-treated sample spectrum within  $\pm 0.2$  °C, the uncertainty in the  
335 SIO-AIS temperature measurement (Beall et al., 2021). A lack of overlap in the 95% binomial  
336 sampling confidence interval within  $\pm 0.2$  °C equates to a significance threshold of  $p < 0.005$   
337 (Krzywinski and Altman, 2013).

338 INP concentrations were additionally measured in 10 SSW samples. For seawater sampling, a  
339 water intake vertical steel pipe was positioned on the starboard of the ship approximately 2 m  
340 below the seasurface level. The seawater was pumped into a 200 L stainless steel tank and  
341 continuously exchanged at a rate of 3000 L h<sup>-1</sup>. SSW samples for INP analysis were collected in  
342 15 mL sterile centrifuge tubes (Falcon™, ThermoFisher Scientific, Waltham, Massachusetts,  
343 USA) and stored frozen at -20 °C until they could be shipped in a dry shipper via Cryoport® (-180  
344 °C) and ultimately stored at -80 °C as for aerosol samples. Heat and hydrogen peroxide treatments  
345 as described above were applied to five of these. To assess the contribution of submicron INPs to



total measured INPs, 2 mL of SSW was filtered through a 0.2  $\mu\text{m}$  sterile syringe-filter (Acrodisc® Pall®, Port Washington, New York, USA) and re-tested.

## 2.5 FLEXPART Back Trajectories

Air mass 72-hour back-trajectories for each sample were simulated using the FLEXible PARTicle dispersion model (FLEXPART) in backward mode (Stohl et al., 1998). NOAA Climate Forecast System (CFS) short-duration ( $t < 6$  h) forecasts (Saha et al., 2014) were used as three-dimensional forcing datasets. Particle releases from 35 m above sea level (ASL) followed the vessel track using vessel position information from the European Common Automatic Weather Station (EUCAWS; <http://eumetnet.eu/>; last access Sept. 2021).

## 3 Results and Discussion

### 3.1 Characteristics of INPs Observed During AQABA

A total of 26 aerosol samples were collected July – August 2017 during AQABA for offline measurements of INPs. The INP concentrations ( $n_{\text{INP}}$ ) measured in samples collected in the Mediterranean Sea, the Red Sea, the Gulf of Aden, Arabian Sea, Gulf of Oman, and Arabian Gulf spanned up to 3 orders of magnitude at  $-15$  °C (Fig. 1). Average ambient dust concentrations during each sampling period ranged from 2–490  $\mu\text{g m}^{-3}$  ( $\text{PM}_{10}$  Table 1). There is no agreed-upon standard for definition of extreme dust events in the literature, though the 24-hr average WHO or US EPA health standards for average  $\text{PM}_{10}$  are commonly used (Gandham et al., 2020; Khaniabadi et al., 2017). Using the US EPA health standard for  $\text{PM}_{10}$  as a threshold for extreme events ( $150 \mu\text{g m}^{-3}$ ), 14 of the 26 samples were collected during dust events. This is conservative given the equivalent WHO guideline for  $\text{PM}_{10}$  is  $50 \mu\text{g m}^{-3}$  (WHO, 2005), in which case 22 of the 26 sampling periods would be classified as dust events. Prior studies have reported comparable  $\text{PM}_{10}$  levels during dust events in the region (Gandham et al., 2020; Krasnov et al., 2016; Shahsavani et al., 2012).

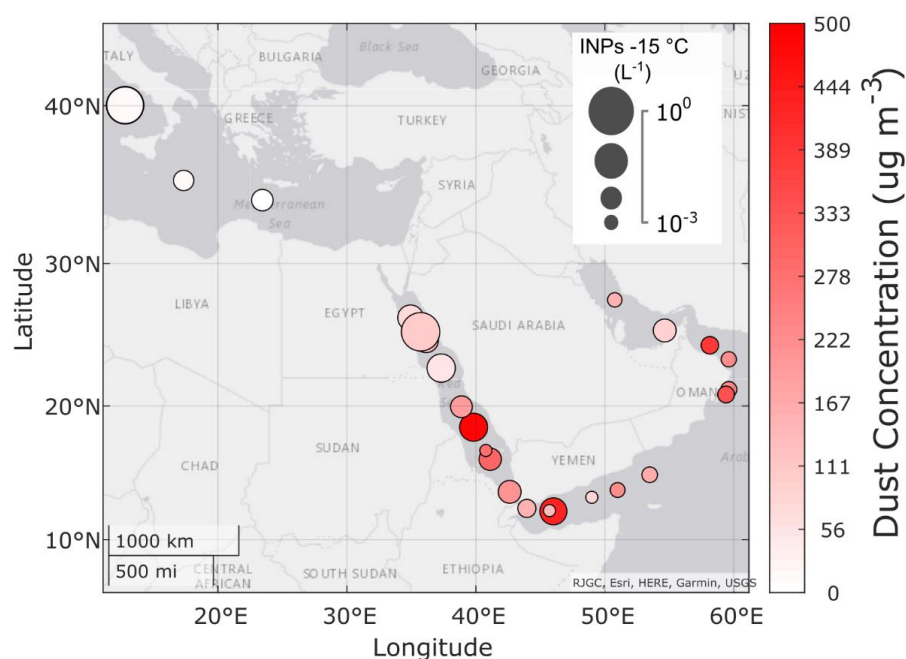
FLEXPART 72-hour air mass back trajectories show that many of samples collected during extreme dust events (f013, f014, f016, f018, and f020) were influenced by emissions from North Africa and the Arabian Peninsula (Figs S8–S9). Other source regions included the Mediterranean,



372 Nile Delta, Sinai Peninsula (f006-f008), Northeast Egypt (f009-f010), Iran (f024), and Southern  
 373 and Eastern Europe (f040, f042, f044).

374

375



376

377 **Figure 1.** Map of the sample locations for 26 aerosol samples collected on the RV *Kommandor*  
 378 *Iona* during Air Quality and climate change in the Arabian BASin (AQABA). Measured INP  
 379 concentrations spanned three orders of magnitude at -15 °C, from  $10^{-3}$  to  $0.5 \text{ L}^{-1}$ . Marker sizes  
 380 indicate abundance of INPs. Marker colors indicate the average ambient dust mass concentration  
 381 during the sampling period from hourly MERRA-2 reanalysis data.



382

383

384

385

386 **Table 1.** Summary of aerosol samples collected during AQABA. “—” indicates where data are missing.

Sample ID	Start datetime (UTC)	Stop datetime (UTC)	Latitude	Longitude	Sample Volume (L air)	Aerosol Surface Area ( $\mu\text{m}^2 \text{cm}^{-3}$ )	Average Dust Concentration ( $\mu\text{g m}^{-3}$ )	Average Seasalt Concentration ( $\mu\text{g m}^{-3}$ )
f006unt	05-Jul 05:46	05-Jul 11:37	26.224	35.025	3370	290	170	-
f007unt	05-Jul 16:40	05-Jul 19:51	26.291	34.933	2588	260	70	-
f008unt	06-Jul 07:09	06-Jul 14:08	25.225	35.775	5225	180	100	-
f009unt	07-Jul 05:50	07-Jul 15:07	25.011	35.947	6940	350	110	-
f010unt	08-Jul 16:33	09-Jul 05:59	23.623	36.931	8073	220	50	-
f013unt	14-Jul 12:26	14-Jul 16:13	18.687	39.672	2283	260	490	10
f014unt	15-Jul 05:10	15-Jul 11:49	16.552	40.834	4000	270	300	5
f016unt	18-Jul 07:04	18-Jul 14:52	11.939	45.334	4690	260	430	-
f018unt	22-Jul 10:20	22-Jul 18:44	20.941	59.474	5025	210	340	-
f019unt	23-Jul 04:48	23-Jul 13:34	21.410	59.691	5270	220	230	-
f020unt	25-Jul 17:15	26-Jul 04:02	23.976	58.809	6511	-	390	5
f023unt	04-Aug 04:05	04-Aug 11:56	28.084	50.284	4720	830	150	4
f024unt	05-Aug 05:57	05-Aug 13:53	25.432	53.853	5221	360	90	-
f025unt	07-Aug 09:26	07-Aug 16:46	23.814	59.186	4410	50	220	12
f030unt	13-Aug 07:08	14-Aug 11:06	15.970	54.705	15111	30	160	-
f031unt	14-Aug 15:03	15-Aug 09:03	14.003	52.357	12972	30	220	-
f032unt	15-Aug 09:42	15-Aug 15:07	13.354	49.432	3260	100	80	6
f033unt	16-Aug 09:30	16-Aug 13:17	12.208	45.706	2280	90	130	2
f034unt	16-Aug 13:27	17-Aug 07:04	12.177	45.429	8464	170	150	1
f035unt	17-Aug 07:30	17-Aug 14:55	13.308	42.974	4460	340	210	2
f036unt	18-Aug 06:36	18-Aug 15:03	16.290	41.038	6634	210	280	2
f037unt	19-Aug 07:05	20-Aug 07:04	18.699	39.609	18806	240	190	7

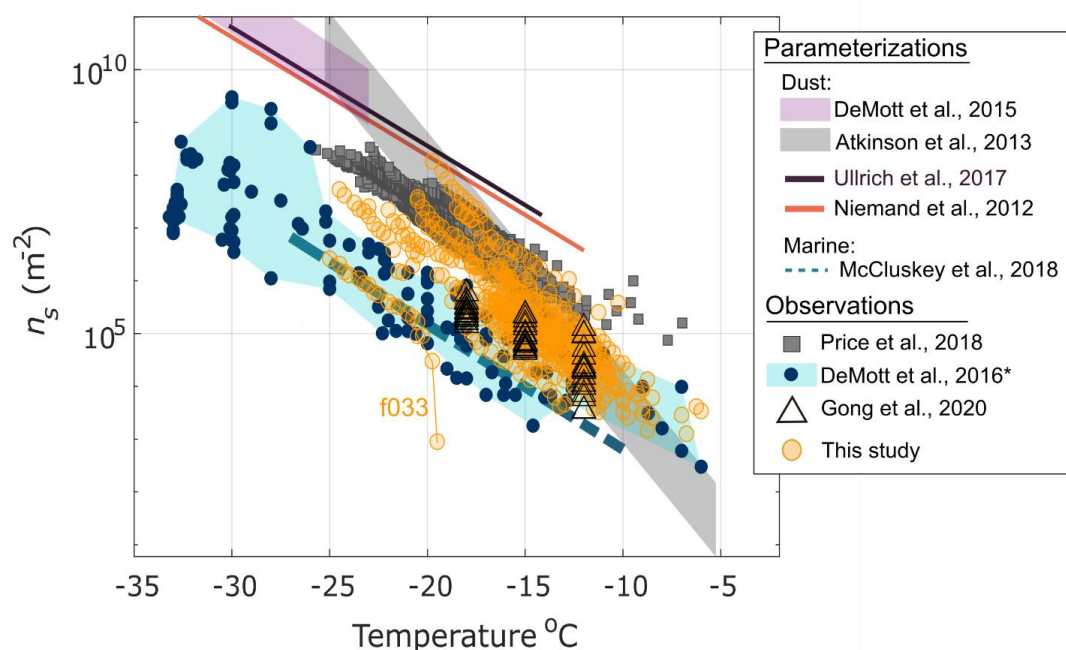




f038unt	21-Aug 07:22	21-Aug 16:01	24.112	36.554	6700	260	140	-
f040unt	26-Aug 16:02	27-Aug 07:04	33.803	24.814	9030	90	<10	3
f042unt	28-Aug 07:51	28-Aug 16:02	35.310	17.965	6396	160	10	2
f044unt	31-Aug 08:30	31-Aug 20:16	39.569	13.380	11296	210	10	-

387

388 In Figure 2, approximated ice nucleation site densities ( $n_s$ ) are compared with multiple population-  
 389 specific observations and parameterizations for dust and marine INPs. The AQABA measurements  
 390 are also compared with observations from dust-laden air over the Tropical Atlantic (Price et al.,  
 391 2018). Overall, observations nearly bridge the full regime between M18, the parameterization for  
 392 marine INPs (McCluskey et al., 2018b), and multiple dust INP parameterizations based on  
 393 laboratory studies of surface dust. At higher temperatures, between -5 and -12 °C, most  
 394 observations show agreement with the composite spectrum of  $n_s$  observed in a range of marine and  
 395 coastal environments from DeMott et al. (2016) and Yang et al. (2019), and/or the Atkinson et al.  
 396 (2013) K-feldspar parameterization. Between -10 and -20 °C, several samples agree with M18  
 397 marine INP parameterization within an order of magnitude, whereas two to three  $n_s$  spectra  
 398 approach the U17 and N12 laboratory-derived dust INP parameterizations within an order of  
 399 magnitude (Niemand et al., 2012; Ullrich et al., 2017), depending on temperature. Multiple  
 400 samples (~8) additionally agreed with Price et al.'s (2018) observations of INPs between 30-3500  
 401 m above the dusty Tropical Atlantic, and most agree with the Gong et al. (2020) surface-level  
 402 observations in the same region (Cabo Verde).



403

404 **Figure 2.** Ice nucleation site densities ( $n_s$ ) as a function of temperature for 25 of 26 aerosol  
 405 samples collected during AQABA. Gong et al. (2020) and Price et al. (2018) measured INPs in  
 406 dust-dominant air masses in the tropical east Atlantic, with minor contributions from SSA, while  
 407 DeMott et al. (2016) measurements were collected across a range of locations and conditions  
 408 within the marine boundary layer comprising air masses mostly dominated by relatively pristine  
 409 marine SSA. INP concentrations measured in sample f033 were below the detection limits  
 410 imposed by field blanks (see Sect. 2.4, Fig. S6). Sample f020 is not shown due to missing aerosol  
 411 surface area data during the sampling period. \*DeMott et al. (2016) data shown have been  
 412 updated with additional data from Yang et al. (2020).

413

414 Considering the frequency of dust events encountered (Table 1), and the high probability that dust  
 415 was the dominant aerosol source during most sampling periods, it is striking that most  $n_s$  spectra  
 416 observed are 1-3 orders of magnitude lower than the values predicted by dust parameterizations.  
 417 As noted in Gong et al. (2020), some deviations could be expected due to the difference between  
 418 approximated  $n_s$  based on total particle surface area in ambient measurements and true  $n_s$  based on



surface area of a homogeneous aerosol population (see Methods Sec. 2.4). The FLEXPART back trajectories show that air masses for multiple samples originated from densely populated regions such as Southern and Eastern Europe (f040, f042, f044, Fig S9). The back trajectories also show that for samples f006-f008, f010, and f038, air masses were influenced by the populous region around the Nile River Delta. Agricultural soil dusts represent a potential constituent of the INPs observed from these regions. A range of  $n_s$  has been reported in studies of agricultural soil dusts, the lower end of which agrees with the  $n_s$  observed in the present study between -8 and -25 °C (Steinke et al., 2016; Tobo et al., 2014; O’Sullivan et al., 2014).

Given the marine environment in which sampling occurred, a significant amount of sea spray aerosol (SSA) was also detected in many of the sampled airmasses (Table 1), and likely present in others for which no composition data were available. Edtbauer et al. (2020) reported the detection of high levels of dimethyl sulfide (DMS, up to 800 ppt) in the Gulf of Aden associated with a local phytoplankton bloom during AQABA (as evidenced by visible bioluminescence around the ship at night) as well as high levels of DMSO<sub>2</sub> and other marine biogenic VOCs from the Somalian upwelling region. As mentioned above, the  $n_s$  for most samples between -6 and -18 °C agree with  $n_s$  derived from observations across various locations within the marine boundary layer (Fig. 2). However, considering that SSA is associated with 1000 times fewer IN sites per unit surface area than dust (i.e. 1000× lower  $n_s$ ) (McCluskey et al., 2018b) and the high relative abundance of dust compared to sea salt concentrations (Table 1), it is unlikely that the observed INPs originated from SSA. In general, detection of marine INPs in ambient aerosol is challenging due to their low relative abundance and decreased efficiency compared to dust (DeMott et al., 2016; McCluskey et al., 2018b). Thus, while SSA contributed to the measured aerosol surface area (Table 1), it is unlikely that the INPs observed in this study were marine in origin, or at least that this is indiscernible in the present study or based on present parameterizations of these populations.

Heterogeneous aerosol composition in the sampled air masses likely contributed to some of the low  $n_s$  spectra observed due to the contribution of non-INPs to the measured aerosol surface area. However, the difference between  $n_s$  observed during the most extreme dust events, i.e., when the aerosol population was likely approaching homogeneity in composition, and the  $n_s$  predicted from N12 and U17 was still greater than 2 orders of magnitude. Figures 3(a) and (b) show overlap in  $n_{INP}$  and  $n_s$  observed in samples collected in low dust and high dust conditions, indicating that the



449 INP populations observed during AQABA exhibited similar efficiencies despite variation in total  
 450 aerosol composition and dust loading. No correlation was found between  $n_{INP}$  and aerosol surface  
 451 area (Fig. S7) or dust concentration. This result is in contrast to Price et al. (2018) who found the  
 452 variability in  $n_{INP}$  to be largely determined by variability in dust loading or aerosol surface area.  
 453 Yet, the aerosol surface area concentrations compare very well, indicative of comparable dustiness  
 454 in the two studies. Excluding three samples Price et al. (2018) collected in an exceptionally  
 455 optically thick dust layer, the average aerosol surface area was  $227 \pm 68 \mu\text{m}^2 \text{cm}^{-3}$  vs.  $226 \pm 26$   
 456  $\mu\text{m}^2 \text{cm}^{-3}$  for the present study. Furthermore, the sample with the highest  $n_s$  at  $-15^\circ\text{C}$  (f040) was  
 457 collected when dust concentrations were lowest ( $2 \mu\text{g m}^{-3}$ ) (Fig. 3, Table 1). This is also in direct  
 458 contrast to Price et al. (2018), who found that the highest  $n_s$  observed corresponded to the highest  
 459 dust loading.

460 Gong et al. (2020) also observed  $n_s$  lower by more than 2 orders of magnitude compared to N12  
 461 and U17 despite the large fraction of supermicron INPs (77-83% depending on temperature), and  
 462 that the supermicron particles were mainly mineral dust. The large differences between  
 463 parameterized  $n_s$  for dust, and  $n_s$  observed in both Gong et al. (2020) and the present study between  
 464  $-12$  and  $-25^\circ\text{C}$  demonstrate that existing  $n_s$ -based parameterizations may not faithfully represent  
 465  $n_s$  at moderate freezing temperatures, despite proximity to major source regions. Whereas DeMott  
 466 et al. (2015a) found that for temperatures  $< -20^\circ\text{C}$ , mineral dust particles from Saharan and Asian  
 467 deserts may be parameterized as a common particle type, our findings suggest that characteristic  
 468  $n_s$  parameterizations for dust from different source regions may be needed  $> -20^\circ\text{C}$ , or,  
 469 alternatively, that this temperature regime requires an alternative to an  $n_s$ -based parameterizations.  
 470 Gong et al. (2019a) demonstrated that predicting  $n_{INP}$  from surface area size distributions alone  
 471 may not be feasible in environments where the aerosol and/or INP composition are unknown and  
 472 proposed a probability density function PDF-based approach to predicting INPs at a given freezing  
 473 temperature.

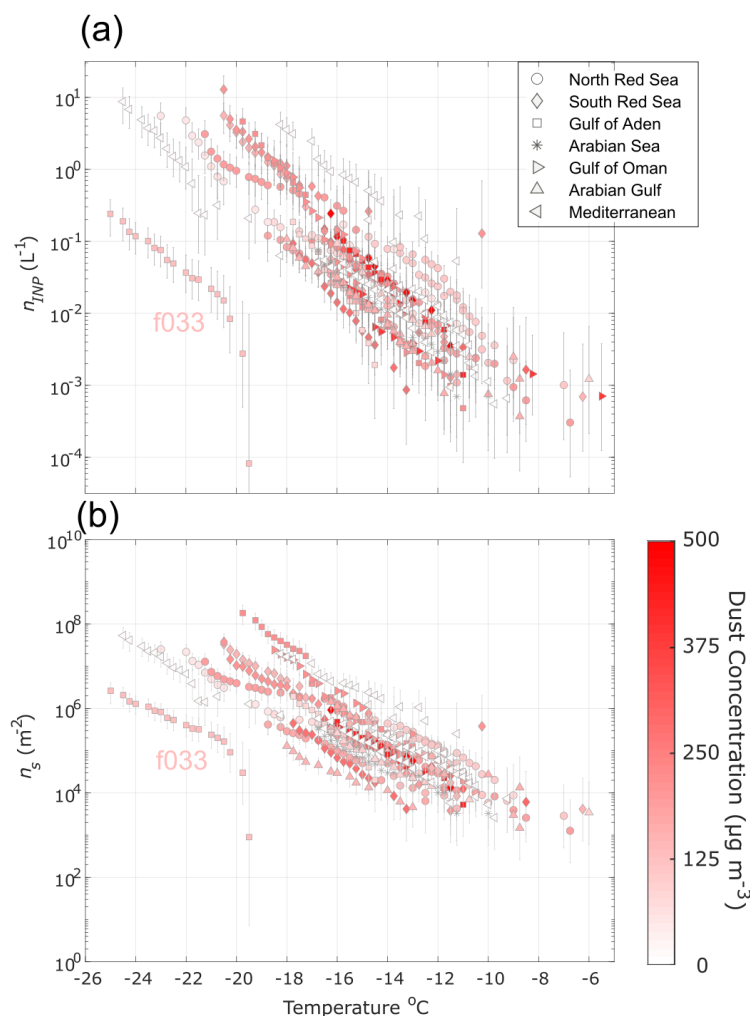


**Figure 3.** INP concentrations ( $n_{\text{INP}}$ ) (a) and ice nucleation site densities ( $n_s$ ) (b) as a function of temperature for 26 aerosol samples collected during AQABA. Markers are colored by the average ambient dust concentration for the respective sampling period. The  $n_s$  measured in samples collected during low dust conditions are equal to or greater than (up to 100×) the  $n_s$  measured during dust events between -9 and -18 °C. INP concentrations measured in sample f033 were below the detection limits imposed by field blanks (see Sect. 2.4, Fig. S6). Sample f020 is not shown in (b) due to missing aerosol surface area data during the sampling period.

Offline treatments for testing heat lability and organic composition of INPs were performed on 12 samples via heat and  $\text{H}_2\text{O}_2$  treatments, respectively (Fig. 4). Prior studies have shown that the IN-



483 active component of various types of mineral dusts are insensitive to heat treatments (Conen et al.,  
484 2011; Hara et al., 2016; Hill et al., 2016; O’Sullivan et al., 2014). The IN activity of K-feldspar,  
485 the dominant IN component of mineral dust, was additionally found to be insensitive to digestion  
486 with peroxide (O’Sullivan et al., 2014). A small number of studies reported degradation of IN  
487 activity with peroxide treatment and/or heat treatment in Arizona Test Dust (ATD), that they  
488 attributed to organic material (Perkins et al., 2020; Yadav et al., 2019). Thus, we assume here that  
489 any degradation of IN activity due to heat and peroxide treatment are due to loss of heat-labile  
490 (e.g. proteinaceous) and heat-stable organic INPs, respectively.

491 Fisher’s Exact Test was applied to frozen and unfrozen well fractions for each untreated sample  
492 and its corresponding treated sample to test for significant differences ( $p < 0.05$ ). Sensitivity to  
493 peroxide in most samples demonstrate the consistent presence of stable organic INPs at  
494 temperatures  $\geq -15$  °C. The lack of peroxide sensitivity at temperatures below  $-15$  °C indicates  
495 dominance by mineral dust INPs at lower temperatures. Heat sensitivity in five samples suggests  
496 that biological INPs contributed to their warmest freezing INPs. Gong et al. (2020) similarly found  
497 heat-sensitivity in INPs at temperatures  $> -10$  °C. Four of the 12 samples exhibited heat sensitivity  
498 at relatively moderate temperatures  $-11$  to  $-18$  °C, including the two samples collected in the  
499 Mediterranean Sea. One sample (f010) exhibited increased INP concentrations in freezing  
500 temperatures below  $-18$  °C after heat and peroxide treatments. That the response to both heat and  
501 peroxide were nearly identical (Fig. 4) suggests that compounds may have been released from the  
502 surface during heating, uncovering a more IN active surface underneath (heating was common to  
503 both procedures). The increased  $n_{INP}$  post heat and peroxide treatment is an unexpected result given  
504 previous studies on treated soil dust measurements (Conen et al., 2011; Hill et al., 2016; O’Sullivan



et al., 2014; Tobo et al., 2014), though an increase in IN activity after peroxide treatment has also been reported in a Himalayan dust sample (Paramonov et al., 2018).

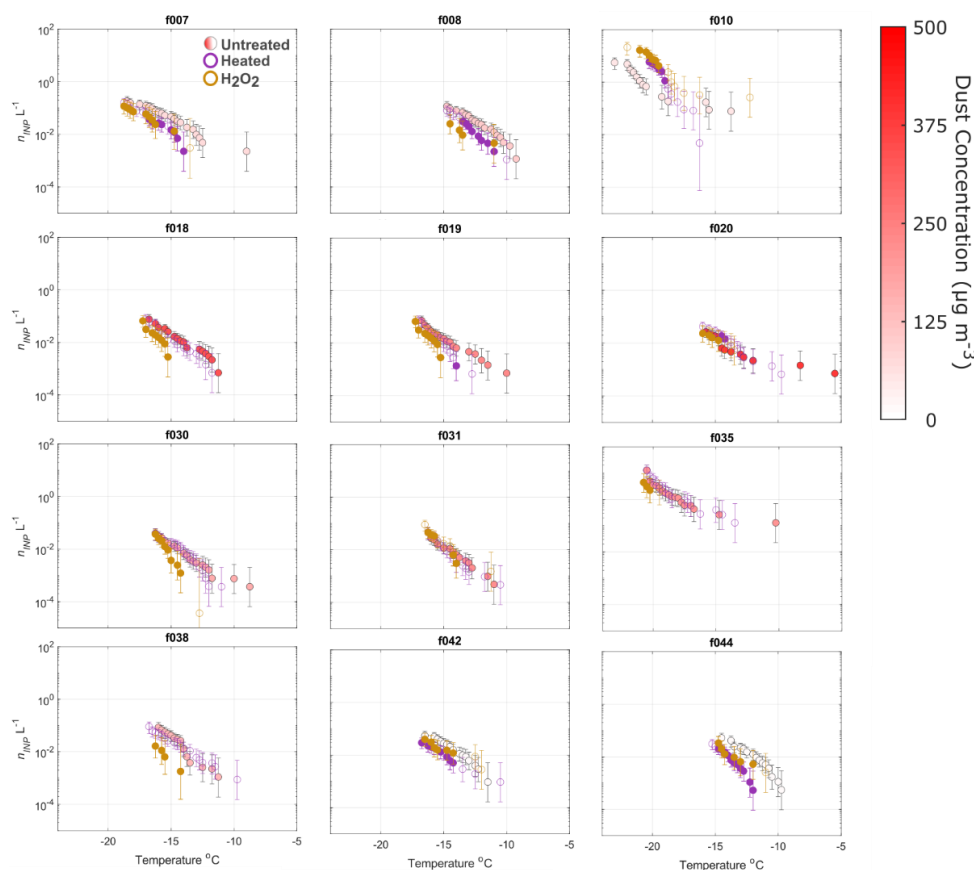


**Figure 4.** INPs in aerosol samples treated with heat and  $\text{H}_2\text{O}_2$  (Methods Sec. 2.4) to test for INP heat-lability and organic composition. Markers of untreated spectra are colored by the average dust concentration during the sampling period. Markers of heat-treated and  $\text{H}_2\text{O}_2$ -treated samples are filled to indicate significant INP concentration difference from untreated samples according to Fisher's Exact Test ( $p < 0.05$ ). Sensitivity to  $\text{H}_2\text{O}_2$  is evident for all samples  $\geq -15^\circ\text{C}$ , indicative of stable organic INPs. Heat-lability is also evident at high to moderate temperatures in multiple samples, demonstrating that biological (e.g., proteinaceous) INPs also contributed to INPs observed during AQABA.

Given the frequency of dust storms and generally high concentrations of dust during most sampling periods, it is surprising that most samples exhibit peroxide sensitivity. Aridisols and entisols are



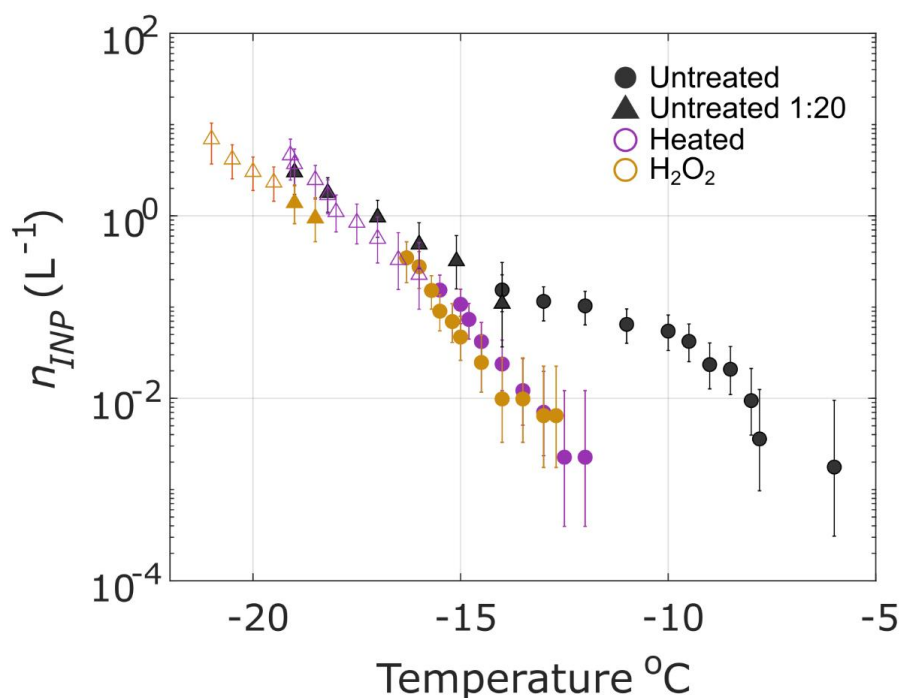


517 the dominant soil types in North Africa and the Arabian Peninsula (Nortcliff, 2012). Both types  
518 are associated with the lowest levels of organic carbon, commonly used as a proxy for total soil  
519 organic matter, compared to other soil types (3 and 9 g kg<sup>-1</sup>, respectively) (Yost and Hartemink,  
520 2019).

521 INP measurements of soil dusts in this region are scarce and have only been reported for a single  
522 surface dust soil sample, sample “SD”, collected 50 km north of Cairo (Niemand et al., 2012). For  
523 comparison with this study, we measured INPs in untreated, heat-treated, and peroxide-treated  
524 subsamples of an archived aliquot of the SD sample described in Niemand et al. (2012). Sample  
525 SD exhibits sensitivity to both heat and peroxide at temperatures > -16 °C, indicating biological  
526 composition of INPs at high freezing temperatures. Multiple AQABA samples influenced by  
527 desert air mass sources show similar sensitivities at higher temperatures: f006, f007, f019, and  
528 f020. Several others exhibit only peroxide-sensitivity in this temperature range. Overall, the heat  
529 and peroxide sensitivities in the SD sample indicate that desert dusts may contribute biological  
530 and/or organic INPs at moderate to high-freezing temperatures, such as those observed in AQABA  
531 samples. Gong et al.'s (2020) results showing heat-sensitivity in INPs at temperatures > -10 °C



532 further demonstrate the contribution of biological INPs at high temperatures in dusty air masses  
 533 near N. Africa.



534

535 **Figure 5.** Measured concentrations of INPs in an aerosolized soil dust sample collected 50 km  
 536 north of Cairo, Egypt, that was treated with heat and peroxide to test for INP heat-lability and  
 537 organic composition, same as in Fig. 4 above (Methods Sec. 2.4). A 1:20 dilution of the sample is  
 538 shown (triangles) and markers of heat-treated and H<sub>2</sub>O<sub>2</sub>-treated samples are filled to indicate  
 539 significant INP concentration differences from untreated samples according to Fisher's Exact Test  
 540 ( $p < 0.05$ ). Sensitivity to peroxide and heat treatments indicates biological INPs between -6 and -  
 541 16 °C.

542 Considering the high freezing temperatures observed, evidence of organic composition, and  
 543 FLEXPART back trajectories showing that aerosol sources included populous regions and at least  
 544 one agriculturally active region (the Nile River Delta), it is possible that agricultural soil dusts  
 545 contributed to some of the relatively higher  $n_s$ ,  $n_{INP}$ , and heat and peroxide sensitivity observed  
 546 during AQABA. Samples from air masses influenced by the Nile River Delta or Southern Europe



(f007-8, f010, f038, f042, f044) show a higher fraction of heat-sensitive INPs (Fig. 4). Heat-sensitivity is indicative of biological INPs, which have been associated with agricultural soil dusts in prior studies (Hill et al., 2016; O’Sullivan et al., 2014). Hill et al. (2016) and O’Sullivan et al. (2014) showed peroxide sensitivity in agricultural soil dusts at temperatures  $> -18$  to  $-15$  °C, respectively, a range which aligns with the peroxide sensitivity exhibited in the present study. Agricultural soil dusts are relatively rich in organic and biological material (Conen et al., 2011, 2016; Ellerbrock et al., 2005; Kögel-Knabner et al., 2008; O’Sullivan et al., 2014) and contribute up to 20-25% of the global dust load (Ginoux et al., 2012). Furthermore, they are associated with IN activities higher than that of mineral dust (Conen et al., 2011; Fornea et al., 2009; Isono and Ikebe, 1960; O’Sullivan et al., 2014; Steinke et al., 2016; Tobo et al., 2014). High onset temperatures, up to  $-6$  °C, are the norm (Conen et al., 2011; Garcia et al., 2012; Hill et al., 2016; O’Sullivan et al., 2014), and the high activity of agricultural soil particles has been attributed to internally mixed organic matter (O’Sullivan et al., 2014; Tobo et al., 2014).

Organic material can condense or adsorb onto aerosols during photochemical and oxidative processes, representing another potential source of organic INPs during AQABA (Dall’Osto et al., 2010; Hinz et al., 2005; Krueger et al., 2004). Could aging explain the organics and decreased  $n_s$  observed? Though dust aerosol was collected within 1 day’s transport from source regions throughout this study, we cannot rule out the possibility of aging impacts, lacking single particle chemistry measurements (e.g., Sullivan et al., 2007). In addition to field observations of INP concentrations demonstrating that aging increased the IN efficiency of desert dust INPs (see Introduction; Boose et al., 2016; Conen et al. 2015), prior studies of the effects of aging on mineral dust INPs have yielded mixed and sometimes contradictory results, indicating that the impact of aging on IN properties likely depends on multiple factors including the ice nucleation pathway, the type of aging process, surface morphology, and mineralogy (Perkins et al., 2020). Multiple studies have investigated the effects of various aging processes on Arizona Test Dust (ATD) as a proxy for diverse natural dust samples. These included exposure to sulfuric acid, nitric acid vapor, and solution-phase processes (Cziczo et al., 2009; Eastwood et al., 2009; Knopf and Koop, 2006; Salam et al., 2007; Sullivan et al., 2010b, 2010a). Perkins et al. (2020) demonstrated the INP lability in ATD through multiple solution-phase aging processes (e.g., incubation in water, exposure to acid or salt), with up to 1000-fold reductions in INP abundance at freezing temperatures  $> 10$  °C. This result contrasts with the increase in IN activity attributed to aging



578 reported in Boose et al. (2016) and Conen et al. (2015). Perkins et al. (2020) additionally reported  
579 that the lability of IN activity in ATD is temperature dependent, with large reductions evident at  
580 freezing temperature  $> 10\text{ }^{\circ}\text{C}$ , yet little to no change at temperatures below  $-15\text{ }^{\circ}\text{C}$ . By contrast,  
581 most of the  $n_s$  spectra in AQABA samples were  $10 - 1000\times$  lower than established dust  
582 parameterizations even at temperatures below  $-15\text{ }^{\circ}\text{C}$ . In summary, it has proven difficult to  
583 determine any consistent impact of atmospheric processing on the IN activity of dust in model  
584 systems such as ATD, and few studies have investigated impacts of aging on ambient desert dust,  
585 especially at modest supercooling. Furthermore, the use of ATD as a proxy for natural dust in INP  
586 studies has been questioned due to the complex IN-properties of natural dust, including mineral  
587 composition and defect sites at the particle surface, the latter of which is likely affected by the  
588 mechanical processing and milling involved in ATD production (e.g., Perkins et al., 2020 and  
589 references therein).

590 The cause of the decreased  $n_s$  observed here and in Gong et al. (2020) compared to dust  $n_s$   
591 parameterizations remains elusive. Both studies were conducted in air masses dominated by dust  
592 near major sources. In contrast, Price et al. (2018) found agreement near the region of the Gong et  
593 al. (2020) study. One obvious difference is that Price et al. (2018) conducted measurements at  
594 higher altitudes, between 30 and 3500 m. A prior study that compared  $n_{INP}$  in dusty air masses at  
595 the surface with  $n_{INP}$  collected between 0.5 and 3 km above sea level found that median  $n_{INP}$   
596 increased by up to  $10\times$  above the surface and correlated to dust loading (Schrod et al., 2017). The  
597 decreased  $n_s$  compared to Price et al. (2018) is also unlikely to be related to differences in INP  
598 measurement. In all three studies, cold stage or droplet assay measurements of immersion mode  
599 INPs were used in resuspensions of aerosol collected on filter samples. Recent studies that  
600 intercompared instruments designed for measurement of immersion mode INPs showed excellent  
601 agreement (i.e., within measurement uncertainty) in measurements of standardized dust and  
602 biological samples (DeMott et al., 2018) and when co-sampling ambient aerosol (DeMott et al.,  
603 2017). Moreover, the DeMott et al. (2018) intercomparison study demonstrated good agreement  
604 in multiple natural dust samples between the various measurement methods used to derive D15,



605 N12 and U17 and the droplet assay methods applied in Gong et al. (2020), Price et al. (2018)),  
 606 and the present study.

607 In light of the evidence from this study that INPs were primarily influenced by organics associated  
 608 with dust, especially at higher temperatures, and the lack of relationship between dust loading,  $n_s$ ,  
 609 and  $n_{INP}$ , we offer the following points for consideration. Prior studies of aerosolized dust  
 610 demonstrated that it is frequently enriched in organic matter (6-20×) and that wind erosion  
 611 selectively removes the chemically-enriched, fine portion of the soil higher of plant nutrients,  
 612 organic matter and metals (Aryal et al., 2012; Delany and Zenchelsky, 1976; Van Pelt and Zobeck,  
 613 2007). Furthermore, a recent study that measured airborne concentrations of prokaryotic cells over  
 614 the Red Sea characterized the region as a “global hot spot” with average concentrations of 155,000  
 615 ( $\pm 65,000$ ), 19× higher than that over the subtropical and tropical open oceans (Mayol et al., 2014;  
 616 Yahya et al., 2019). Yahya et al. (2019) demonstrated that the microbial loading was very likely  
 617 related to the high concentrations of dust, as 99.9% of the cells were attached to dust particles.  
 618 Organic and biological species have been shown to dominate IN activity at temperatures  $> \sim -15$   
 619 °C in many studies (e.g., Kanji et al., 2017; Ladino et al., 2019; O’Sullivan et al., 2018). Thus, a  
 620 faithful representation of dust INPs may require two parameterizations: one for the IN activity  
 621 dominated by minerals  $< \sim -15$  °C such as D15, U17 and N12, and another for the dust-associated  
 622 organics  $> \sim -15$  °C. As IN-active organics are limited compared to the IN-active mineral  
 623 component of dust, we could expect an increase in  $n_s$  slope between warm and cold regimes. The  
 624 apparent decreased  $n_s$  observed in this study between -18 and -12 °C could potentially be related  
 625 to a plateau in  $n_s$  through the transition between the mineral and organic “modes” (see Fig. 5). This  
 626 study underscores the need to characterize the IN-active organic species associated with dust from  
 627 major source regions and to investigate the extent to which biological and/or organic particles  
 628 contribute to INP populations in dust-laden air masses at high to moderate freezing temperatures.

### 629 3.2 Seawater Source Potential

630 The  $n_{INP}$  values in 10 SSW samples collected during AQABA were used to characterize the INP  
 631 source potential of SSA generated by bubble bursting (Wang et al., 2017). Results from prior  
 632 studies have demonstrated that jet droplets are a more efficient transfer vehicle than film drops of  
 633 INPs into SSA particles (Mitts et al., 2021; Wang et al., 2017). While it is unlikely that many of

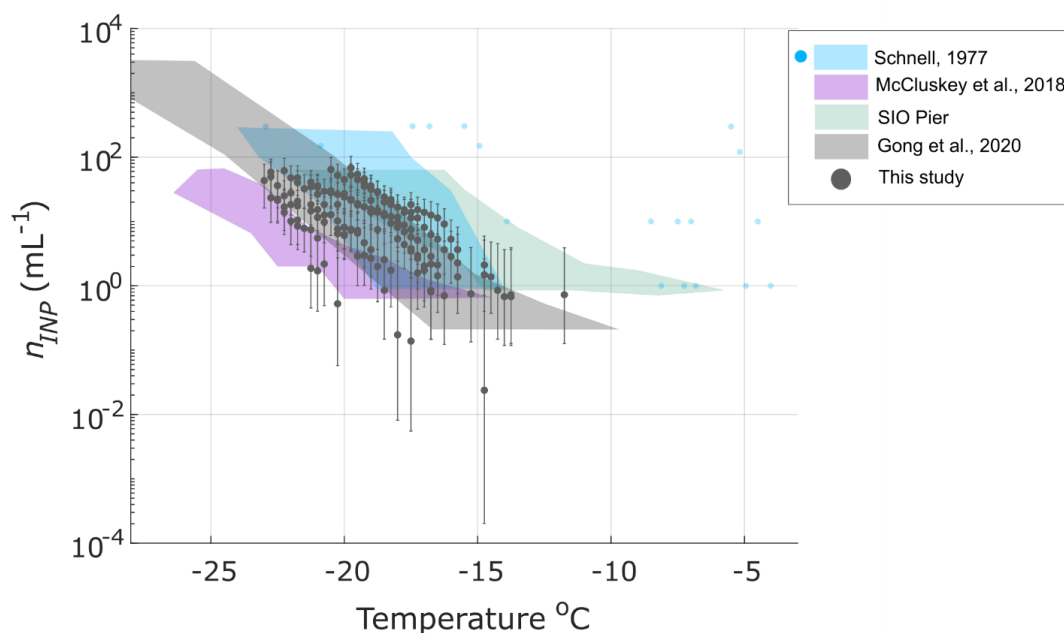


634 the INPs detected in aerosol samples were marine in origin (see Sec. 3.1), we measured the INP  
635 concentrations in SSW to test whether the seawater source strength was comparable to that of  
636 prior studies, or were possibly enriched with INPs due to biological activity or even dust  
637 deposition (Cornwell et al., 2020).

638 Figure S10 shows how the INP concentrations measured at -19 °C in 10 seawater samples varied  
639 by the sample collection location. Concentrations ranged between 1 and 50 INPs mL<sup>-1</sup> and were  
640 highest between the Gulf of Oman and the Gulf of Aden. This region exhibited relatively high  
641 chlorophyll *a* during the cruise, with levels between 1 and 30 mg m<sup>-3</sup> (Fig. S11). In Fig. 6, INP  
642 concentrations were compared with SSW from the Ellen Browning Scripps Memorial Pier in  
643 coastal Southern California (SIO Pier), Cabo Verde in the Northeast Atlantic, the Southern  
644 Ocean (McCluskey et al., 2017), and the Northwest Atlantic (Schnell, 1977). AQABA INP  
645 concentrations were most comparable with Gong et al.'s (2020) observations in Cabo Verde. The



646 lack of any unusually high INP spectra suggests that INP enrichment due to dust deposition  
 647 (Cornwell et al. 2020) was absent or infrequent.



648

649 **Figure 6.** Measured INP concentrations in 10 SSW samples collected during AQABA. Also  
 650 shown are the composite INP spectrum of coastal SSW samples collected on São Vicente  
 651 Island, Cabo Verde (Gong et al., 2020), coastal SSW samples collected at the Ellen Browning  
 652 Scripps Pier (green shading), and SSW samples collected in the Southern Ocean (McCluskey et  
 653 al., 2018c). Schnell's (1977) SSW measurements are represented as a composite spectrum of 24  
 654 samples (blue shaded region) and 5 additional spectra (blue markers) from samples that exhibited  
 655 higher freezing temperatures. All spectra presented are uncorrected for freezing point depression.

656 Offline treatments for testing heat lability, organic composition, and size were applied to 5 of the  
 657 10 seawater samples (Methods Sec. 2.4). Heat and 0.2  $\mu\text{m}$  filtering treatments suggest that a  
 658 large fraction of the seawater INPs were heat sensitive and larger than 0.2  $\mu\text{m}$ . These results are  
 659 indicative of the particulate organic carbon (POC) type of marine INP defined in McCluskey et  
 660 al. (2018a) (Fig. S12). Heat-resilience but peroxide-sensitivity in sample s001 additionally  
 661 indicates the presence of non-proteinaceous organic INPs, such as the dissolved organic carbon





(DOC) type defined in McCluskey et al. (2018a). Considering the characteristically low IN activity of the SSW, the lower  $n_s$  of SSA compared to mineral dust (McCluskey et al., 2018b), and the frequency of dust events during AQABA, our findings suggest that dust was highly likely to be the dominant INP class observed in this study.

#### 4 Conclusions

Observations from the two-month AQABA campaign in the Mediterranean, Red Sea, Arabian Sea and Arabian Gulf are among the first INP measurements made in close proximity to the two largest dust sources globally: the Sahara and the Arabian Peninsula (Kok et al., 2021). INP concentrations spanned two or more orders of magnitude ( $0.002$  to  $0.5 \text{ L}^{-1}$  at  $-15 \text{ }^\circ\text{C}$ ).

In summary, INPs observed during AQABA were very likely dominated by mineral dust with some additional contributions possibly from densely-populated and/or agricultural regions including the Nile River Delta region and Southern or Eastern Europe. Despite proximity to major dust sources and a high frequency of dust events with mass concentrations up to  $490 \mu\text{g m}^{-3}$  ( $\text{PM}_{10}$ ), the observed  $n_s$  for most samples was lower by 1-3 orders of magnitude compared to  $n_s$  predicted by dust parametrizations N12 and U17 at  $T < -12 \text{ }^\circ\text{C}$  (Niemand et al., 2012; Ullrich et al., 2017). Many INPs measured in AQABA showed agreement with the A13 parameterization for K-feldspar (Atkinson et al., 2013), an ice-active component of desert dust, with observations within the marine boundary layer (DeMott et al., 2016; Yang et al., 2020), and with the Price et al.'s (2018) measurements of INP concentrations in dust-laden air masses over the Tropical Atlantic. Peroxide sensitivity was evident in all samples tested (12 of 26), at temperatures  $\geq -15 \text{ }^\circ\text{C}$ , demonstrating a consistent contribution of organic material to warm-temperature INPs. Heat-sensitivity further suggested the presence of biological (e.g., proteinaceous) INPs in a subset of samples, particularly at high freezing temperatures. While the dominant mineral dusts in the region are associated with the lowest concentrations of soil organic carbon globally (e.g., Yost and Hartemink, 2019 and references therein), aerosolized fine dust is known to be enriched in organic matter (Aryal et al., 2012; Delany and Zenchelsky, 1976; Van Pelt and Zobeck, 2007) and is additionally associated with high microbial loading in the Red Sea (Yahya et al., 2019). A soil dust sample from North Africa exhibited heat and peroxide sensitivity between  $-5$  and  $-16 \text{ }^\circ\text{C}$ , further demonstrating that the IN activity of mineral dust could be associated with organic and/or biological material.



691 Contrary to Price et al. (2018), who measured INP in the dust-laden Tropical Atlantic, no  
692 correlation was found between dust loading and  $n_{INP}$  or  $n_s$ . Results from this study and Gong et al.  
693 (2020) indicate that the existing  $n_s$  parameterizations alone do not skillfully represent mineral dust  
694 associated INPs at modest supercooling near major dust sources.

695 The source strengths of Red Sea, Mediterranean, Arabian Sea, and Arabian Gulf bulk seawater  
696 were also evaluated. The maximum source potential was observed in the Arabian Sea (50 INP  
697  $\text{mL}^{-1}$  at  $-19^\circ\text{C}$ .) Overall, the observed  $n_{INP}$  range agreed well with the Gong et al. (2020) SSW  
698 measurements at Cabo Verde.

699 Considering that desert dust parameterizations overpredicted the  $n_s$  values observed during  
700 AQABA, despite proximity to major global emissions sources, this study demonstrates the need  
701 to evaluate the fidelity of dust INP parameterizations in nascent versus aged dust populations. The  
702 discrepancies underscore the challenges of evaluating dust-specific INP parameterizations: limited  
703 observations at modest supercooling, few assured methods for distinguishing between different  
704 INP sources in ambient aerosol, a dearth of characteristic soil dust samples from major dust  
705 sources, and limited knowledge of the specific composition and characteristics of dust INPs at  
706 temperatures  $> -15^\circ\text{C}$ .

707 In addition to providing observations at high to moderate freezing temperatures, future studies  
708 could apply the methods developed in Gong et al. (2020) to estimate the contribution of marine  
709 INPs to the aerosol sampled. Furthermore, given the combination of marine, dust, and  
710 anthropogenically-influenced air masses encountered, and the evidence of organic and biological  
711 INPs at modest supercooling in this study and Gong et al. (2020), future studies could benefit from  
712 advances in on-line Light-Induced Fluorescence (LIF) measurement techniques. Whereas the  
713 interpretation of fluorescence data from most LIF-based instruments has been limited by the lack  
714 of spectroscopic information, newer instruments support real-time spectrally-resolved size and  
715 fluorescence measurement information for single particles (Fennelly et al., 2018; Huffman et al.,  
716 2020; Könemann et al., 2019). This information could be used to “tag” different classes of organics  
717 and biological aerosols, enabling investigations of relationships between  $n_s$ ,  $n_{INP}$  and organic  
718 signatures in, e.g., mineral dusts and agricultural soil dusts. Finally, the decreased  $n_s$  observed in  
719 this study further motivate comprehensive aerosol-ice nucleation studies, which aim to achieve  
720 closure between measured and predicted ambient INP concentrations by simultaneously



721 characterizing ambient INPs and ice nucleation relevant properties of the total aerosol population,  
722 such as composition and aerosol chemical mixing state (Sullivan et al., 2007).

723 **Data Availability:** The data set supporting this manuscript is hosted by the UCSD Library  
724 Digital Collections (<https://doi.org/10.6075/J0X0676P>) (Beall et al., 2021).

725 **Author contributions:**

726 CMB, TCH, PJD, MOA, CP, JL, JS, FD, BW, HH, MDS, and KAP designed the study. CMB  
727 performed the INP measurements, FLEXPART modeling and analysis with support from TCH,  
728 PJD, MOA, MDS, MP and KAP. TCH, PJD and MOA contributed significantly to the writing,  
729 preparation of figures and analysis. TK, MI, RP and HH supported the field collection of aerosol  
730 for INP analysis and TK additionally provided aerosol number concentration data. JS and MP  
731 provided aerosol water-soluble composition data. FD oversaw the aerosol sizing and AMS  
732 composition measurements and analysis. All authors contributed to the writing of the article.

733 **Competing interests:**

734 The authors declare they have no conflict of interest.

735

736 **Acknowledgements:**

737 The authors acknowledge collaborations with King Abdullah University of Science and  
738 Technology (KAUST), the Cyprus Institute (CyI) and the Kuwait Institute for Scientific  
739 Research (KISR). We additionally thank Marcel Dorf and Claus Koeppel for the organization of  
740 the campaign, as well as Horst Fischer, Ivan Tadic and Uwe Parchatka for provision of the NO  
741 data. Analyses and visualizations of dust mass concentrations and Chl *a* used in this paper were  
742 produced with the Giovanni online data system, developed and maintained by the NASA GES  
743 DISC. Maps throughout this article were created using ArcGIS® software by Esri. We would also like  
744 to thank Hays Ships Ltd. and the *Kommandor Iona*'s crew for their attention to the safety and  
745 well-being of the researchers. Funding was provided by Highly Cited Program at King Saud  
746 University and the Max Planck Society and the University of California San Diego (UCSD)  
747 Understanding and Protecting the Planet initiative.



748

749

750 **References**

- 751 Agresti, A. and Coull, B. A.: Approximate Is Better than “Exact” for Interval Estimation of Binomial  
752 Proportions, *Am. Stat.*, 52(2), 119, doi:10.2307/2685469, 1998.
- 753 Ardon-Dryer, K. and Levin, Z.: Ground-based measurements of immersion freezing in the eastern  
754 Mediterranean, *Atmos. Chem. Phys.*, 14(10), 5217–5231, doi:10.5194/acp-14-5217-2014, 2014.
- 755 Aryal, R., Kandel, D., Acharya, D., Chong, M. N. and Beecham, S.: Unusual Sydney dust storm and its  
756 mineralogical and organic characteristics, *Environ. Chem.*, 9(6), 537–546 [online] Available from:  
757 <https://doi.org/10.1071/EN12131>, 2012.
- 758 Atkinson, J. D., Murray, B. J., Woodhouse, M. T., Whale, T. F., Baustian, K. J., Carslaw, K. S., Dobbie,  
759 S., O’Sullivan, D. and Malkin, T. L.: The importance of feldspar for ice nucleation by mineral dust in  
760 mixed-phase clouds, *Nature*, 498(7454), 355–358, doi:10.1038/nature12278, 2013.
- 761 Beall, C. M., Stokes, M. D., Hill, T. C., DeMott, P. J., DeWald, J. T. and Prather, K. A.: Automation and  
762 Heat Transfer Characterization of Immersion Mode Spectroscopy for Analysis of Ice Nucleating  
763 Particles, *Atmos. Meas. Tech.*, (February), 1–25, doi:10.5194/amt-2016-412, 2017.
- 764 Beall, C. M., Michaud, J. M., Fish, M. A., Dinasquet, J., Cornwell, G. C., Stokes, M. D., Burkart, M. D.,  
765 Hill, T. C., Demott, P. J. and Prather, K. A.: Cultivable halotolerant ice-nucleating bacteria and fungi in  
766 coastal precipitation, *Atmos. Chem. Phys.*, 21(11), 9031–9045, doi:10.5194/acp-21-9031-2021, 2021.
- 767 Boose, Y., Sierau, B., Isabel García, M., Rodríguez, S., Alastuey, A., Linke, C., Schnaiter, M.,  
768 Kupiszewski, P., Kanji, Z. A. and Lohmann, U.: Ice nucleating particles in the Saharan Air Layer, *Atmos.*  
769 *Chem. Phys.*, 16(14), 9067–9087, doi:10.5194/acp-16-9067-2016, 2016.
- 770 Bourtsoukidis, E., Ernle, L., Crowley, J. N., Lelieveld, J., Paris, J.-D., Pozzer, A., Walter, D. and  
771 Williams, J.: Non-methane hydrocarbon ( $\text{C}_2$ – $\text{C}_8$ ) sources and sinks around the  
772 Arabian Peninsula, *Atmos. Chem. Phys.*, 19(10), 7209–7232, doi:10.5194/acp-19-7209-2019, 2019.
- 773 Bourtsoukidis, E., Pozzer, A., Sattler, T., Matthaios, V. N., Ernle, L., Edtbauer, A., Fischer, H.,  
774 Könemann, T., Osipov, S., Paris, J.-D., Pfannerstill, E. Y., Stönnner, C., Tadic, I., Walter, D., Wang, N.,  
775 Lelieveld, J. and Williams, J.: The Red Sea Deep Water is a potent source of atmospheric ethane and  
776 propane, *Nat. Commun.*, 11(1), 447, doi:10.1038/s41467-020-14375-0, 2020.



- 777 Broadley, S. L., Murray, B. J., Herbert, R. J., Atkinson, J. D., Dobbie, S., Malkin, T. L., Condliffe, E. and  
 778 Neve, L.: Immersion mode heterogeneous ice nucleation by an illite rich powder representative of  
 779 atmospheric mineral dust, *Atmos. Chem. Phys.*, 12(1), 287–307, doi:10.5194/acp-12-287-2012, 2012.
- 780 Buchard, V., Randles, C. A., da Silva, A. M., Darmenov, A., Colarco, P. R., Govindaraju, R., Ferrare, R.,  
 781 Hair, J., Beyersdorf, A. J., Ziemba, L. D. and Yu, H.: The MERRA-2 Aerosol Reanalysis, 1980 Onward.  
 782 Part II: Evaluation and Case Studies, *J. Clim.*, 30(17), 6851–6872, doi:10.1175/JCLI-D-16-0613.1, 2017.
- 783 Burrows, S. M., Hoose, C., Pöschl, U. and Lawrence, M. G.: Ice nuclei in marine air: biogenic particles or  
 784 dust?, *Atmos. Chem. Phys.*, 13(1), 245–267, doi:10.5194/acp-13-245-2013, 2013.
- 785 Celik, S., Drewnick, F., Fachinger, F., Brooks, J., Darbyshire, E., Coe, H., Paris, J.-D., Eger, P. G.,  
 786 Schuladen, J., Tadic, I., Friedrich, N., Dienhart, D., Hottmann, B., Fischer, H., Crowley, J. N., Harder, H.  
 787 and Borrmann, S.: Influence of vessel characteristics and atmospheric processes on the gas and particle  
 788 phase of ship emission plumes: in situ measurements in the Mediterranean Sea and around the Arabian  
 789 Peninsula, *Atmos. Chem. Phys.*, 20(8), 4713–4734, doi:10.5194/acp-20-4713-2020, 2020.
- 790 Chin, M., Ginoux, P., Kinne, S., Torres, O., Holben, B. N., Duncan, B. N., Martin, R. V., Logan, J. A.,  
 791 Higurashi, A. and Nakajima, T.: Tropospheric Aerosol Optical Thickness from the GOCART Model and  
 792 Comparisons with Satellite and Sun Photometer Measurements, *J. Atmos. Sci.*, 59(3), 461–483,  
 793 doi:10.1175/1520-0469(2002)059<0461:TAOTFT>2.0.CO;2, 2002.
- 794 Colarco, P., da Silva, A., Chin, M. and Diehl, T.: Online simulations of global aerosol distributions in the  
 795 NASA GEOS-4 model and comparisons to satellite and ground-based aerosol optical depth, *J. Geophys.*  
 796 *Res. Atmos.*, 115(D14), doi:https://doi.org/10.1029/2009JD012820, 2010.
- 797 Conen, F., Morris, C. E., Leifeld, J., Yakutin, M. V and Alewell, C.: Biological residues define the ice  
 798 nucleation properties of soil dust, *Atmos. Chem. Phys.*, 11(18), 9643–9648, doi:10.5194/acp-11-9643-  
 799 2011, 2011.
- 800 Conen, F., Rodríguez, S., Hüglin, C., Henne, S., Herrmann, E., Bukowiecki, N. and Alewell, C.:  
 801 Atmospheric ice nuclei at the high-altitude observatory Jungfraujoch, Switzerland, *Tellus, Ser. B Chem.*  
 802 *Phys. Meteorol.*, 67(1), 1–10, doi:10.3402/tellusb.v67.25014, 2015.
- 803 Conen, F., Stopelli, E. and Zimmermann, L.: Clues that decaying leaves enrich Arctic air with ice  
 804 nucleating particles, *Atmos. Environ.*, 129, 91–94, doi:10.1016/j.atmosenv.2016.01.027, 2016.
- 805 Cornwell, G. C., McCluskey, C. S., Levin, E. J. T., Suski, K. J., DeMott, P. J., Kreidenweis, S. M. and  
 806 Prather, K. A.: Direct Online Mass Spectrometry Measurements of Ice Nucleating Particles at a California



- 807 Coastal Site, *J. Geophys. Res. Atmos.*, 124(22), 12157–12172, doi:doi:10.1029/2019JD030466, 2019.
- 808 Cornwell, G. C., Sultana, C. M., Prank, M., Cochran, R. E., Hill, T. C. J., Schill, G. P., DeMott, P. J.,  
 809 Mahowald, N. and Prather, K. A.: Ejection of Dust From the Ocean as a Potential Source of Marine Ice  
 810 Nucleating Particles, *J. Geophys. Res. Atmos.*, 125(24), e2020JD033073,  
 811 doi:https://doi.org/10.1029/2020JD033073, 2020.
- 812 Cziczo, D. J., Froyd, K. D., Gallavardin, S. J., Moehler, O., Benz, S., Saathoff, H. and Murphy, D. M.:  
 813 Deactivation of ice nuclei due to atmospherically relevant surface coatings, *Environ. Res. Lett.*, 4(4),  
 814 44013, doi:10.1088/1748-9326/4/4/044013, 2009.
- 815 Dall'Osto, M., Harrison, R. M., Highwood, E. J., O'Dowd, C., Ceburnis, D., Querol, X. and Achterberg,  
 816 E. P.: Variation of the mixing state of Saharan dust particles with atmospheric transport, *Atmos. Environ.*,  
 817 44(26), 3135–3146, doi:https://doi.org/10.1016/j.atmosenv.2010.05.030, 2010.
- 818 Delany, A. C. and Zenchelsky, S.: THE ORGANIC COMPONENT OF WIND-EROSION-  
 819 GENERATED SOIL-DERIVED AEROSOL, *Soil Sci.*, 121(3) [online] Available from:  
 820 https://journals.lww.com/soilsci/Fulltext/1976/03000/THE\_ORGANIC\_COMPONENT\_OF\_WIND\_ER  
 821 OSION\_GENERATED.2.aspx, 1976.
- 822 Demott, P. J., Prenni, A. J., Mcmeeking, G. R., Sullivan, R. C., Petters, M. D., Tobo, Y., Niemand, M.,  
 823 Möhler, O., Snider, J. R., Wang, Z. and Kreiden: Integrating laboratory and field data to quantify the  
 824 immersion freezing ice nucleation activity of mineral dust particles, , 393–409, doi:10.5194/acp-15-393-  
 825 2015, 2015.
- 826 DeMott, P. J., Hill, T. C. J., McCluskey, C. S., Prather, K. A., Collins, D. B., Sullivan, R. C., Ruppel, M.  
 827 J., Mason, R. H., Irish, V. E., Lee, T., Hwang, C. Y., Rhee, T. S., Snider, J. R., McMeeking, G. R.,  
 828 Dhaniyala, S., Lewis, E. R., Wentzell, J. J. B., Abbatt, J., Lee, C., Sultana, C. M., Ault, A. P., Axson, J.  
 829 L., Diaz Martinez, M., Venero, I., Santos-Figueroa, G., Stokes, M. D., Deane, G. B., Mayol-Bracero, O.  
 830 L., Grassian, V. H., Bertram, T. H., Bertram, A. K., Moffett, B. F. and Franc, G. D.: Sea spray aerosol as  
 831 a unique source of ice nucleating particles, *Proc. Natl. Acad. Sci.*, 113(21), 5797–5803,  
 832 doi:10.1073/pnas.1514034112, 2016.
- 833 DeMott, P. J., Hill, T. C. J., Petters, M. D., Bertram, A. K., Tobo, Y., Mason, R. H., Suski, K. J.,  
 834 McCluskey, C. S., Levin, E. J. T., Schill, G. P., Boose, Y., Rauker, A. M., Miller, A. J., Zaragoza, J.,  
 835 Rocci, K., Rothfuss, N. E., Taylor, H. P., Hader, J. D., Chou, C., Huffman, J. A., Pöschl, U., Prenni, A. J.  
 836 and Kreidenweis, S. M.: Comparative measurements of ambient atmospheric concentrations of ice  
 837 nucleating particles using multiple immersion freezing methods and a continuous flow diffusion chamber,



- 838 Atmos. Chem. Phys., 17(18), 11227–11245, doi:10.5194/acp-17-11227-2017, 2017.
- 839 DeMott, P. J., Möhler, O., Cziczo, D. J., Hiranuma, N., Petters, M. D., Petters, S. S., Belosi, F.,  
 840 Bingemer, H. G., Brooks, S. D., Budke, C., Burkert-Kohn, M., Collier, K. N., Danielczok, A., Eppers, O.,  
 841 Felgitsch, L., Garimella, S., Grothe, H., Herenz, P., Hill, T. C. J., Höhler, K., Kanji, Z. A., Kiselev, A.,  
 842 Koop, T., Kristensen, T. B., Krüger, K., Kulkarni, G., Levin, E. J. T., Murray, B. J., Nicosia, A.,  
 843 O’Sullivan, D., Peckhaus, A., Polen, M. J., Price, H. C., Reicher, N., Rothenberg, D. A., Rudich, Y.,  
 844 Santachiara, G., Schiebel, T., Schrod, J., Seifried, T. M., Stratmann, F., Sullivan, R. C., Suski, K. J.,  
 845 Szakáll, M., Taylor, H. P., Ullrich, R., Vergara-Temprado, J., Wagner, R., Whale, T. F., Weber, D., Welti,  
 846 A., Wilson, T. W., Wolf, M. J. and Zenker, J.: The Fifth International Workshop on Ice Nucleation phase  
 847 2 (FIN-02): laboratory intercomparison of ice nucleation measurements, Atmos. Meas. Tech., 11(11),  
 848 6231–6257, doi:10.5194/amt-11-6231-2018, 2018.
- 849 Eastwood, M. L., Cremel, S., Wheeler, M., Murray, B. J., Girard, E. and Bertram, A. K.: Effects of  
 850 sulfuric acid and ammonium sulfate coatings on the ice nucleation properties of kaolinite particles,  
 851 Geophys. Res. Lett., 36(2), doi:https://doi.org/10.1029/2008GL035997, 2009.
- 852 Edtbauer, A., Stönnner, C., Pfannerstill, E. Y., Berasategui, M., Walter, D., Crowley, J. N., Lelieveld, J.  
 853 and Williams, J.: A new marine biogenic emission: methane sulfonamide (MSAM), dimethyl sulfide  
 854 (DMS), and dimethyl sulfone ( $\text{CH}_3\text{SOCH}_3$ ) measured in air over the Arabian Sea, Atmos. Chem.  
 855 Phys., 20(10), 6081–6094, doi:10.5194/acp-20-6081-2020, 2020.
- 856 Eger, P. G., Friedrich, N., Schuladen, J., Shenolikar, J., Fischer, H., Tadic, I., Harder, H., Martinez, M.,  
 857 Rohloff, R., Tauer, S., Drewnick, F., Fachinger, F., Brooks, J., Darbyshire, E., Sciare, J., Pikridas, M.,  
 858 Lelieveld, J. and Crowley, J. N.: Shipborne measurements of  $\text{ClNO}_2$  in the Mediterranean Sea and  
 859 around the Arabian Peninsula during summer, Atmos. Chem. Phys., 19(19), 12121–12140,  
 860 doi:10.5194/acp-19-12121-2019, 2019.
- 861 Ellerbrock, R. H., Gerke, H. H., Bachmann, J. and Goebel, M.-O.: Composition of Organic Matter  
 862 Fractions for Explaining Wettability of Three Forest Soils, Soil Sci. Soc. Am. J., 69(1), 57–66,  
 863 doi:https://doi.org/10.2136/sssaj2005.0057, 2005.
- 864 Fennelly, M. J., Sewell, G., Prentice, M. B., O’Connor, D. J. and Sodeau, J. R.: Review: The Use of Real-  
 865 Time Fluorescence Instrumentation to Monitor Ambient Primary Biological Aerosol Particles (PBAP),  
 866 Atmosphere (Basel), 9(1), doi:10.3390/atmos9010001, 2018.
- 867 Fornea, A. P., Brooks, S. D., Dooley, J. B. and Saha, A.: Heterogeneous freezing of ice on atmospheric  
 868 aerosols containing ash, soot, and soil, J. Geophys. Res. Atmos., 114(D13),





- 869 doi:https://doi.org/10.1029/2009JD011958, 2009.
- 870 Friedrich, N., Eger, P., Shenolikar, J., Sobanski, N., Schuladen, J., Dienhart, D., Hottmann, B., Tadic, I.,  
 871 Fischer, H., Martinez, M., Rohloff, R., Tauer, S., Harder, H., Pfannerstill, E. Y., Wang, N., Williams, J.,  
 872 Brooks, J., Drewnick, F., Su, H., Li, G., Cheng, Y., Lelieveld, J. and Crowley, J. N.: Reactive nitrogen  
 873 around the Arabian Peninsula and in the Mediterranean Sea during the 2017 AQABA ship campaign,  
 874 Atmos. Chem. Phys., 21(10), 7473–7498, doi:10.5194/acp-21-7473-2021, 2021.
- 875 Gandham, H., Dasari, H. P., Langodan, S., Karumuri, R. K. and Hoteit, I.: Major Changes in Extreme  
 876 Dust Events Dynamics Over the Arabian Peninsula During 2003–2017 Driven by Atmospheric  
 877 Conditions, J. Geophys. Res. Atmos., 125(24), e2020JD032931,  
 878 doi:https://doi.org/10.1029/2020JD032931, 2020.
- 879 Garcia, E., Hill, T. C. J., Prenni, A. J., DeMott, P. J., Franc, G. D. and Kreidenweis, S. M.: Biogenic ice  
 880 nuclei in boundary layer air over two U.S. High Plains agricultural regions, J. Geophys. Res. Atmos.,  
 881 117(D18), doi:https://doi.org/10.1029/2012JD018343, 2012.
- 882 Gelaro, R., McCarty, W., Suárez, M. J., Todling, R., Molod, A., Takacs, L., Randles, C. A., Darmenov,  
 883 A., Bosilovich, M. G., Reichle, R., Wargan, K., Coy, L., Cullather, R., Draper, C., Akella, S., Buchard,  
 884 V., Conaty, A., da Silva, A. M., Gu, W., Kim, G.-K., Koster, R., Lucchesi, R., Merkova, D., Nielsen, J.  
 885 E., Partyka, G., Pawson, S., Putman, W., Rienecker, M., Schubert, S. D., Sienkiewicz, M. and Zhao, B.:  
 886 The Modern-Era Retrospective Analysis for Research and Applications, Version 2 (MERRA-2), J. Clim.,  
 887 30(14), 5419–5454, doi:10.1175/JCLI-D-16-0758.1, 2017.
- 888 Ginoux, P., Chin, M., Tegen, I., Prospero, J. M., Holben, B., Dubovik, O. and Lin, S.-J.: Sources and  
 889 distributions of dust aerosols simulated with the GOCART model, J. Geophys. Res. Atmos., 106(D17),  
 890 20255–20273, doi:https://doi.org/10.1029/2000JD000053, 2001.
- 891 Ginoux, P., Prospero, J. M., Gill, T. E., Hsu, N. C. and Zhao, M.: Global-scale attribution of  
 892 anthropogenic and natural dust sources and their emission rates based on MODIS Deep Blue aerosol  
 893 products, Rev. Geophys., 50(3), doi:https://doi.org/10.1029/2012RG000388, 2012.
- 894 Gong, X., Wex, H., Müller, T., Wiedensohler, A., Höhler, K., Kandler, K., Ma, N., Dietel, B., Schiebel,  
 895 T., Möhler, O. and Stratmann, F.: Characterization of aerosol properties at Cyprus, focusing on cloud  
 896 condensation nuclei and ice-nucleating particles, Atmos. Chem. Phys., 19(16), 10883–10900,  
 897 doi:10.5194/acp-19-10883-2019, 2019a.
- 898 Gong, X., Wex, H., van Pinxteren, M., Triesch, N., Fomba, K. W., Lubitz, J., Stolle, C., Robinson, T.-B.,  
 899 Müller, T., Herrmann, H. and Stratmann, F.: Ice nucleating particles measured in air, cloud and seawater



- 900 at the Cape Verde Atmospheric Observatory (CVAO), , doi:10.1594/PANGAEA.906946, 2019b.
- 901 Gong, X., Wex, H., van Pinxteren, M., Triesch, N., Fomba, K. W., Lubitz, J., Stolle, C., Robinson, T.-B.,  
 902 Müller, T., Herrmann, H. and Stratmann, F.: Characterization of aerosol particles at Cabo Verde close to  
 903 sea level and at the cloud level -- Part 2: Ice-nucleating particles in air, cloud and seawater, *Atmos. Chem.*  
 904 *Phys.*, 20(3), 1451–1468, doi:10.5194/acp-20-1451-2020, 2020.
- 905 Hara, K., Maki, T., Kakikawa, M., Kobayashi, F. and Matsuki, A.: Effects of different temperature  
 906 treatments on biological ice nuclei in snow samples, *Atmos. Environ.*, 140, 415–419,  
 907 doi:10.1016/j.atmosenv.2016.06.011, 2016.
- 908 Harrison, A. D., Whale, T. F., Carpenter, M. A., Holden, M. A., Neve, L., O’Sullivan, D., Vergara  
 909 Temprado, J. and Murray, B. J.: Not all feldspars are equal: a survey of ice nucleating properties across  
 910 the feldspar group of minerals, *Atmos. Chem. Phys.*, 16(17), 10927–10940, doi:10.5194/acp-16-10927-  
 911 2016, 2016.
- 912 Harrison, A. D., Lever, K., Sanchez-Marroquin, A., Holden, M. A., Whale, T. F., Tarn, M. D., McQuaid,  
 913 J. B. and Murray, B. J.: The ice-nucleating ability of quartz immersed in water and its atmospheric  
 914 importance compared to K-feldspar, *Atmos. Chem. Phys.*, 19(17), 11343–11361, doi:10.5194/acp-19-  
 915 11343-2019, 2019.
- 916 Hartmann, M., Adachi, K., Eppers, O., Haas, C., Herber, A., Holzinger, R., Hünerbein, A., Jäkel, E.,  
 917 Jentzsch, C., van Pinxteren, M., Wex, H., Willmes, S. and Stratmann, F.: Wintertime Airborne  
 918 Measurements of Ice Nucleating Particles in the High Arctic: A Hint to a Marine, Biogenic Source for Ice  
 919 Nucleating Particles, *Geophys. Res. Lett.*, 47(13), e2020GL087770,  
 920 doi:https://doi.org/10.1029/2020GL087770, 2020.
- 921 Hill, T. C. J., DeMott, P. J., Tobo, Y., Fröhlich-Nowoisky, J., Moffett, B. F., Franc, G. D. and  
 922 Kreidenweis, S. M.: Sources of organic ice nucleating particles in soils, *Atmos. Chem. Phys.*, 16(11),  
 923 7195–7211, doi:10.5194/acp-16-7195-2016, 2016.
- 924 Hinz, K.-P., Trimborn, A., Weingartner, E., Henning, S., Baltensperger, U. and Spengler, B.: Aerosol  
 925 single particle composition at the Jungfraujoch, *J. Aerosol Sci.*, 36(1), 123–145,  
 926 doi:https://doi.org/10.1016/j.jaerosci.2004.08.001, 2005.
- 927 Hoose, C. and Möhler, O.: Heterogeneous ice nucleation on atmospheric aerosols: A review of results  
 928 from laboratory experiments., 2012.
- 929 Hoose, C., Kristjánsson, J. E., Chen, J.-P. and Hazra, A.: A Classical-Theory-Based Parameterization of



- 930 Heterogeneous Ice Nucleation by Mineral Dust, Soot, and Biological Particles in a Global Climate Model,  
 931 J. Atmos. Sci., 67(8), 2483–2503, doi:10.1175/2010JAS3425.1, 2010.
- 932 Huffman, J. A., Perring, A. E., Savage, N. J., Clot, B., Crouzy, B., Tummon, F., Shoshanim, O., Damit,  
 933 B., Schneider, J., Sivaprakasam, V., Zawadowicz, M. A., Crawford, I., Gallagher, M., Topping, D.,  
 934 Doughty, D. C., Hill, S. C. and Pan, Y.: Real-time sensing of bioaerosols: Review and current  
 935 perspectives, Aerosol Sci. Technol., 54(5), 465–495, doi:10.1080/02786826.2019.1664724, 2020.
- 936 Huneus, N., Schulz, M., Balkanski, Y., Griesfeller, J., Prospero, J., Kinne, S., Bauer, S., Boucher, O.,  
 937 Chin, M., Dentener, F., Diehl, T., Easter, R., Fillmore, D., Ghan, S., Ginoux, P., Grini, A., Horowitz, L.,  
 938 Koch, D., Krol, M. C., Landing, W., Liu, X., Mahowald, N., Miller, R., Morcrette, J.-J., Myhre, G.,  
 939 Penner, J., Perlwitz, J., Stier, P., Takemura, T. and Zender, C. S.: Global dust model intercomparison in  
 940 AeroCom phase I, Atmos. Chem. Phys., 11(15), 7781–7816, doi:10.5194/acp-11-7781-2011, 2011.
- 941 Isono, K. and Ikebe, Y.: On the Ice-nucleating Ability of Rock-forming Minerals and Soil  
 942 Particles&lowast;, J. Meteorol. Soc. Japan. Ser. II, 38(5), 213–230, doi:10.2151/jmsj1923.38.5\_213,  
 943 1960.
- 944 Kanji, Z. A., Ladino, L. A., Wex, H., Boose, Y., Burkert-Kohn, M., Cziczo, D. J. and Krämer, M.:  
 945 Overview of Ice Nucleating Particles, Meteorol. Monogr., 58, 1.1-1.33, doi:10.1175/amsmonographs-d-  
 946 16-0006.1, 2017.
- 947 Khaniabadi, Y. O., Daryanoosh, S. M., Amrane, A., Polosa, R., Hopke, P. K., Goudarzi, G., Mohammadi,  
 948 M. J., Sicard, P. and Armin, H.: Impact of Middle Eastern Dust storms on human health, Atmos. Pollut.  
 949 Res., 8(4), 606–613, doi:https://doi.org/10.1016/j.apr.2016.11.005, 2017.
- 950 Kinne, S., Schulz, M., Textor, C., Guibert, S., Balkanski, Y., Bauer, S. E., Bernsten, T., Berglen, T. F.,  
 951 Boucher, O., Chin, M., Collins, W., Dentener, F., Diehl, T., Easter, R., Feichter, J., Fillmore, D., Ghan,  
 952 S., Ginoux, P., Gong, S., Grini, A., Hendricks, J., Herzog, M., Horowitz, L., Isaksen, I., Iversen, T.,  
 953 Kirkevåg, A., Kloster, S., Koch, D., Kristjansson, J. E., Krol, M., Lauer, A., Lamarque, J. F., Lesins, G.,  
 954 Liu, X., Lohmann, U., Montanaro, V., Myhre, G., Penner, J., Pitari, G., Reddy, S., Seland, O., Stier, P.,  
 955 Takemura, T. and Tie, X.: An AeroCom initial assessment – optical properties in aerosol component  
 956 modules of global models, Atmos. Chem. Phys., 6(7), 1815–1834, doi:10.5194/acp-6-1815-2006, 2006.
- 957 Kleist, D. T., Parrish, D. F., Derber, J. C., Treadon, R., Wu, W.-S. and Lord, S.: Introduction of the GSI  
 958 into the NCEP Global Data Assimilation System, Weather Forecast., 24(6), 1691–1705,  
 959 doi:10.1175/2009WAF2222201.1, 2009.
- 960 Klingmüller, K., Pozzer, A., Metzger, S., Stenchikov, G. L. and Lelieveld, J.: Aerosol optical depth trend



- 961 over the Middle East, *Atmos. Chem. Phys.*, 16(8), 5063–5073, doi:10.5194/acp-16-5063-2016, 2016.
- 962 Knopf, D. A. and Koop, T.: Heterogeneous nucleation of ice on surrogates of mineral dust, *J. Geophys.*  
 963 *Res. Atmos.*, 111(D12), doi:https://doi.org/10.1029/2005JD006894, 2006.
- 964 Kögel-Knabner, I., Guggenberger, G., Kleber, M., Kandeler, E., Kalbitz, K., Scheu, S., Eusterhues, K.  
 965 and Leinweber, P.: Organo-mineral associations in temperate soils: Integrating biology, mineralogy, and  
 966 organic matter chemistry, *J. Plant Nutr. Soil Sci.*, 171(1), 61–82,  
 967 doi:https://doi.org/10.1002/jpln.200700048, 2008.
- 968 Kok, J. F., Adebisi, A. A., Albani, S., Balkanski, Y., Checa-Garcia, R., Chin, M., Colarco, P. R.,  
 969 Hamilton, D. S., Huang, Y., Ito, A., Klose, M., Li, L., Mahowald, N. M., Miller, R. L., Obiso, V., Pérez  
 970 Garc\'ia-Pando, C., Rocha-Lima, A. and Wan, J. S.: Contribution of the world's main dust source regions  
 971 to the global cycle of desert dust, *Atmos. Chem. Phys.*, 21(10), 8169–8193, doi:10.5194/acp-21-8169-  
 972 2021, 2021.
- 973 Könnemann, T., Savage, N., Klimach, T., Walter, D., Fröhlich-Nowoisky, J., Su, H., Pöschl, U., Huffman,  
 974 J. A. and Pöhlker, C.: Spectral Intensity Bioaerosol Sensor (SIBS): an instrument for spectrally resolved  
 975 fluorescence detection of single particles in real time, *Atmos. Meas. Tech.*, 12(2), 1337–1363,  
 976 doi:10.5194/amt-12-1337-2019, 2019.
- 977 Krasnov, H., Katra, I. and Friger, M.: Increase in dust storm related PM<sub>10</sub> concentrations: A time series  
 978 analysis of 2001–2015, *Environ. Pollut.*, 213, 36–42, doi:https://doi.org/10.1016/j.envpol.2015.10.021,  
 979 2016.
- 980 Krueger, B. J., Grassian, V. H., Cowin, J. P. and Laskin, A.: Heterogeneous chemistry of individual  
 981 mineral dust particles from different dust source regions: the importance of particle mineralogy, *Atmos.*  
 982 *Environ.*, 38(36), 6253–6261, doi:https://doi.org/10.1016/j.atmosenv.2004.07.010, 2004.
- 983 Krzywinski, M. and Altman, N.: Error bars, *Nat. Methods*, 10(10), 921–922, doi:10.1038/nmeth.2659,  
 984 2013.
- 985 Ladino, L. A., Raga, G. B., Alvarez-Ospina, H., Andino-Enríquez, M. A., Rosas, I., Martínez, L.,  
 986 Salinas, E., Miranda, J., Ramírez-Díaz, Z., Figueroa, B., Chou, C., Bertram, A. K., Quintana, E. T.,  
 987 Maldonado, L. A., García-Reynoso, A., Si, M. and Irish, V. E.: Ice-nucleating particles in a coastal  
 988 tropical site, *Atmos. Chem. Phys.*, 19(9), 6147–6165, doi:10.5194/acp-19-6147-2019, 2019.
- 989 Lohmann, U. and Feichter, J.: Global indirect aerosol effects: a review, *Atmos. Chem. Phys.*, 5(3), 715–  
 990 737, doi:10.5194/acp-5-715-2005, 2005.



- 991 Manders, A. M. ., Schapp, M., Jozwicka, M., van Arkel, F., Weijers, E. . and Matthijssen, J.: The  
 992 contribution of sea salt to PM<sub>10</sub> and PM in the Netherlands, [online] Available from:  
 993 <http://www.pbl.nl/sites/default/files/cms/publicaties/500099004.pdf>, 2009.
- 994 Mayol, E., Jiménez, M. A., Herndl, G. J., Duarte, C. M. and Arrieta, J. M.: Resolving the abundance and  
 995 air-sea fluxes of airborne microorganisms in the North Atlantic Ocean, *Front. Microbiol.*, 5, 557,  
 996 doi:10.3389/fmicb.2014.00557, 2014.
- 997 McCluskey, C. S., Hill, T. C. J., Malfatti, F., Sultana, C. M., Lee, C., Santander, M. V., Beall, C. M.,  
 998 Moore, K. A., Cornwell, G. C., Collins, D. B., Prather, K. A., Jayarathne, T., Stone, E. A., Azam, F.,  
 999 Kreidenweis, S. M. and DeMott, P. J.: A Dynamic Link between Ice Nucleating Particles Released in  
 1000 Nascent Sea Spray Aerosol and Oceanic Biological Activity during Two Mesocosm Experiments, *J.*  
 1001 *Atmos. Sci.*, 74(1), 151–166, doi:10.1175/JAS-D-16-0087.1, 2017.
- 1002 McCluskey, C. S., Hill, T. C. J., Sultana, C. M., Laskina, O., Trueblood, J., Santander, M. V., Beall, C.  
 1003 M., Michaud, J. M., Kreidenweis, S. M., Prather, K. A., Grassian, V. and DeMott, P. J.: A Mesocosm  
 1004 Double Feature: Insights into the Chemical Makeup of Marine Ice Nucleating Particles, *J. Atmos. Sci.*,  
 1005 75(7), 2405–2423, doi:10.1175/JAS-D-17-0155.1, 2018a.
- 1006 McCluskey, C. S., Ovadnevaite, J., Rinaldi, M., Atkinson, J., Belosi, F., Ceburnis, D., Marullo, S., Hill,  
 1007 T. C. J., Lohmann, U., Kanji, Z. A., O'Dowd, C., Kreidenweis, S. M. and DeMott, P. J.: Marine and  
 1008 Terrestrial Organic Ice-Nucleating Particles in Pristine Marine to Continentally Influenced Northeast  
 1009 Atlantic Air Masses, *J. Geophys. Res. Atmos.*, 123(11), 6196–6212, doi:10.1029/2017JD028033, 2018b.
- 1010 McCluskey, C. S., Hill, T. C. J., Humphries, R. S., Rauker, A. M., Moreau, S., Strutton, P. G., Chambers,  
 1011 S. D., Williams, A. G. and McRobert, I.: Observations of Ice Nucleating Particles Over Southern Ocean  
 1012 Waters, *Geophys. Res. Lett.*, 989–997, doi:10.1029/2018GL079981, 2018c.
- 1013 Mitts, B., Wang, X., Lucero, D., Beall, C., Deane, G., DeMott, P. and Prather, K.: Importance of  
 1014 Supermicron Ice Nucleating Particles in Nascent Sea Spray, *Geophys. Res. Lett.*, n/a(n/a),  
 1015 e2020GL089633, doi:https://doi.org/10.1029/2020GL089633, 2021.
- 1016 Molod, A., Takacs, L., Suarez, M. and Bacmeister, J.: Development of the GEOS-5 atmospheric general  
 1017 circulation model: evolution from MERRA to MERRA2, *Geosci. Model Dev.*, 8(5), 1339–1356,  
 1018 doi:10.5194/gmd-8-1339-2015, 2015.
- 1019 Murray, B. J., O'Sullivan, D., Atkinson, J. D. and Webb, M. E.: Ice nucleation by particles immersed in  
 1020 supercooled cloud droplets., *Chem. Soc. Rev.*, 41(19), 6519–54, doi:10.1039/c2cs35200a, 2012.



- 1021 Nickovic, S., Vukovic, A., Vujadinovic, M., Djurdjevic, V. and Pejanovic, G.: Technical Note: High-  
 1022 resolution mineralogical database of dust-productive soils for atmospheric dust modeling, *Atmos. Chem.*  
 1023 *Phys.*, 12(2), 845–855, doi:10.5194/acp-12-845-2012, 2012.
- 1024 Niedermeier, D., Augustin-Bauditz, S., Hartmann, S., Wex, H., Ignatius, K. and Stratmann, F.: Can we  
 1025 define an asymptotic value for the ice active surface site density for heterogeneous ice nucleation?, *J.*  
 1026 *Geophys. Res. Atmos.*, 120(10), 5036–5046, doi:https://doi.org/10.1002/2014JD022814, 2015.
- 1027 Niemand, M., Möhler, O., Vogel, B., Vogel, H., Hoose, C., Connolly, P., Klein, H., Bingemer, H.,  
 1028 Demott, P., Skrotzki, J. and Leisner, T.: A particle-surface-area-based parameterization of immersion  
 1029 freezing on desert dust particles, *J. Atmos. Sci.*, 69(10), 3077–3092, doi:10.1175/JAS-D-11-0249.1, 2012.
- 1030 Nortcliff, S.: *World Soil Resources and Food Security*. Edited by R. Lal and BA Stewart. Boca Raton, FL,  
 1031 USA: CRC Press (2012), pp. 574, £82.00. ISBN-13: 978-1439844502., *Exp. Agric.*, 48(2), 305–306,  
 1032 2012.
- 1033 O’Sullivan, D., Murray, B. J., Malkin, T. L., Whale, T. F., Umo, N. S., Atkinson, J. D., Price, H. C.,  
 1034 Baustian, K. J., Browse, J. and Webb, M. E.: Ice nucleation by fertile soil dusts: relative importance of  
 1035 mineral and biogenic components, *Atmos. Chem. Phys.*, 14(4), 1853–1867, doi:10.5194/acp-14-1853-  
 1036 2014, 2014.
- 1037 O’Sullivan, D., Adams, M. P., Tarn, M. D., Harrison, A. D., Vergara-Temprado, J., Porter, G. C. E.,  
 1038 Holden, M. A., Sanchez-Marroquin, A., Carotenuto, F., Whale, T. F., McQuaid, J. B., Walshaw, R.,  
 1039 Hedges, D. H. P., Burke, I. T., Cui, Z. and Murray, B. J.: Contributions of biogenic material to the  
 1040 atmospheric ice-nucleating particle population in North Western Europe, *Sci. Rep.*, 8(1), 13821,  
 1041 doi:10.1038/s41598-018-31981-7, 2018.
- 1042 Paramonov, M., David, R. O., Kretzschmar, R. and Kanji, Z. A.: A laboratory investigation of the ice  
 1043 nucleation efficiency of three types of mineral and soil dust, *Atmos. Chem. Phys.*, 18(22), 16515–16536,  
 1044 doi:10.5194/acp-18-16515-2018, 2018.
- 1045 Van Pelt, R. S. and Zobeck, T. M.: Chemical Constituents of Fugitive Dust, *Environ. Monit. Assess.*,  
 1046 130(1), 3–16, doi:10.1007/s10661-006-9446-8, 2007.
- 1047 Perkins, R. J., Gillette, S. M., Hill, T. C. J. and DeMott, P. J.: The Labile Nature of Ice Nucleation by  
 1048 Arizona Test Dust, *ACS Earth Sp. Chem.*, 4(1), 133–141, doi:10.1021/acsearthspacechem.9b00304,  
 1049 2020.
- 1050 Pfannerstill, E. Y., Wang, N., Edtbauer, A., Bourtsoukidis, E., Crowley, J. N., Dienhart, D., Eger, P. G.,



- 1051 Ernle, L., Fischer, H., Hottmann, B., Paris, J.-D., Stönnner, C., Tadic, I., Walter, D., Lelieveld, J. and  
 1052 Williams, J.: Shipborne measurements of total OH reactivity around the Arabian Peninsula and its role in  
 1053 ozone chemistry, *Atmos. Chem. Phys.*, 19(17), 11501–11523, doi:10.5194/acp-19-11501-2019, 2019.
- 1054 Price, H. C., Baustian, K. J., McQuaid, J. B., Blyth, A., Bower, K. N., Choularton, T., Cotton, R. J., Cui,  
 1055 Z., Field, P. R., Gallagher, M., Hawker, R., Merrington, A., Miltenberger, A., Neely III, R. R., Parker, S.  
 1056 T., Rosenberg, P. D., Taylor, J. W., Trembath, J., Vergara-Temprado, J., Whale, T. F., Wilson, T. W.,  
 1057 Young, G. and Murray, B. J.: Atmospheric Ice-Nucleating Particles in the Dusty Tropical Atlantic, *J.*  
 1058 *Geophys. Res. Atmos.*, 123(4), 2175–2193, doi:https://doi.org/10.1002/2017JD027560, 2018.
- 1059 Rienecker, M. M., Suarez, M. J., Gelaro, R., Todling, R., Bacmeister, J., Liu, E., Bosilovich, M. G.,  
 1060 Schubert, S. D., Takacs, L., Kim, G.-K., Bloom, S., Chen, J., Collins, D., Conaty, A., da Silva, A., Gu,  
 1061 W., Joiner, J., Koster, R. D., Lucchesi, R., Molod, A., Owens, T., Pawson, S., Pegion, P., Redder, C. R.,  
 1062 Reichle, R., Robertson, F. R., Ruddick, A. G., Sienkiewicz, M. and Woollen, J.: MERRA: NASA's  
 1063 Modern-Era Retrospective Analysis for Research and Applications, *J. Clim.*, 24(14), 3624–3648,  
 1064 doi:10.1175/JCLI-D-11-00015.1, 2011.
- 1065 Saha, S., Moorthi, S., Wu, X., Wang, J., Nadiga, S., Tripp, P., Behringer, D., Hou, Y.-T., Chuang, H.,  
 1066 Iredell, M., Ek, M., Meng, J., Yang, R., Mendez, M. P., van den Dool, H., Zhang, Q., Wang, W., Chen,  
 1067 M. and Becker, E.: The NCEP Climate Forecast System Version 2, *J. Clim.*, 27(6), 2185–2208,  
 1068 doi:10.1175/JCLI-D-12-00823.1, 2014.
- 1069 Salam, A., Lohmann, U. and Lesins, G.: Ice nucleation of ammonia gas exposed montmorillonite mineral  
 1070 dust particles, *Atmos. Chem. Phys.*, 7(14), 3923–3931, doi:10.5194/acp-7-3923-2007, 2007.
- 1071 Schnell, R. C.: Ice Nuclei in Seawater, Fog Water and Marine Air off the Coast of Nova Scotia: Summer  
 1072 1975, *J. Atmos. Sci.*, 34(8), 1299–1305, doi:10.1175/1520-0469(1977)034<1299:INISFW>2.0.CO;2,  
 1073 1977.
- 1074 Schrod, J., Weber, D., Drücke, J., Keleshis, C., Pikridas, M., Ebert, M., Cvetković, B., Nickovic, S.,  
 1075 Marinou, E., Baars, H., Ansmann, A., Vrekoussis, M., Mihalopoulos, N., Sciare, J., Curtius, J. and  
 1076 Bingemer, H. G.: Ice nucleating particles over the Eastern Mediterranean measured by unmanned aircraft  
 1077 systems, *Atmos. Chem. Phys.*, 17(7), 4817–4835, doi:10.5194/acp-17-4817-2017, 2017.
- 1078 Shahsavani, A., Naddafi, K., Jafarzade Haghighifard, N., Mesdaghinia, A., Yunesian, M., Nabizadeh, R.,  
 1079 Arahani, M., Sowlat, M. H., Yarahmadi, M., Saki, H., Alimohamadi, M., Nazmara, S., Motevalian, S. A.  
 1080 and Goudarzi, G.: The evaluation of PM<sub>10</sub>, PM<sub>2.5</sub>, and PM<sub>1</sub> concentrations during the Middle Eastern  
 1081 Dust (MED) events in Ahvaz, Iran, from april through september 2010, *J. Arid Environ.*, 77, 72–83,





- 1082 doi:https://doi.org/10.1016/j.jaridenv.2011.09.007, 2012.
- 1083 Steinke, I., Funk, R., Busse, J., Iturri, A., Kirchen, S., Leue, M., Möhler, O., Schwartz, T., Schnaiter, M.,  
1084 Sierau, B., Toprak, E., Ullrich, R., Ulrich, A., Hoose, C. and Leisner, T.: Ice nucleation activity of  
1085 agricultural soil dust aerosols from Mongolia, Argentina, and Germany, *J. Geophys. Res. Atmos.*,  
1086 121(22), 13,513–559,576, doi:https://doi.org/10.1002/2016JD025160, 2016.
- 1087 Stohl, A., Hittenberger, M. and Wotawa, G.: Validation of the Lagrangian particle dispersion model  
1088 FLEXPART against large scale tracer experiment data, *Atmos. Environ.*, 32(24), 4245–4264, 1998.
- 1089 Sullivan, R. C., Guazzotti, S. A., Sodeman, D. A. and Prather, K. A.: Direct observations of the  
1090 atmospheric processing of Asian mineral dust, *Atmos. Chem. Phys.*, 7(5), 1213–1236, doi:10.5194/acp-7-  
1091 1213-2007, 2007.
- 1092 Sullivan, R. C., Miñambres, L., DeMott, P. J., Prenni, A. J., Carrico, C. M., Levin, E. J. T. and  
1093 Kreidenweis, S. M.: Chemical processing does not always impair heterogeneous ice nucleation of mineral  
1094 dust particles, *Geophys. Res. Lett.*, 37(24), doi:https://doi.org/10.1029/2010GL045540, 2010a.
- 1095 Sullivan, R. C., Petters, M. D., DeMott, P. J., Kreidenweis, S. M., Wex, H., Niedermeier, D., Hartmann,  
1096 S., Clauss, T., Stratmann, F., Reitz, P., Schneider, J. and Sierau, B.: Irreversible loss of ice nucleation  
1097 active sites in mineral dust particles caused by sulphuric acid condensation, *Atmos. Chem. Phys.*, 10(23),  
1098 11471–11487, doi:10.5194/acp-10-11471-2010, 2010b.
- 1099 Suski, K. J., Hill, T. C. J., Levin, E. J. T., Miller, A., DeMott, P. J. and Kreidenweis, S. M.: Agricultural  
1100 harvesting emissions of ice-nucleating particles, *Atmos. Chem. Phys.*, 18(18), 13755–13771,  
1101 doi:10.5194/acp-18-13755-2018, 2018.
- 1102 Tadic, I., Crowley, J. N., Dienhart, D., Eger, P., Harder, H., Hottmann, B., Martinez, M., Parchatka, U.,  
1103 Paris, J.-D., Pozzer, A., Rohloff, R., Schuladen, J., Shenolikar, J., Tauer, S., Lelieveld, J. and Fischer, H.:  
1104 Net ozone production and its relationship to nitrogen oxides and volatile organic compounds in the  
1105 marine boundary layer around the Arabian Peninsula, *Atmos. Chem. Phys.*, 20(11), 6769–6787,  
1106 doi:10.5194/acp-20-6769-2020, 2020.
- 1107 Tobo, Y., DeMott, P. J., Hill, T. C. J., Prenni, A. J., Swoboda-Colberg, N. G., Franc, G. D. and  
1108 Kreidenweis, S. M.: Organic matter matters for ice nuclei of agricultural soil origin, *Atmos. Chem. Phys.*,  
1109 14(16), 8521–8531, doi:10.5194/acp-14-8521-2014, 2014.
- 1110 Ullrich, R., Hoose, C., Möhler, O., Niemand, M., Wagner, R., Höhler, K., Hiranuma, N., Saathoff, H. and  
1111 Leisner, T.: A new ice nucleation active site parameterization for desert dust and soot, *J. Atmos. Sci.*,





- 1112 74(3), 699–717, doi:10.1175/JAS-D-16-0074.1, 2017.
- 1113 Vergara-Temprado, J., Murray, B. J., Wilson, T. W., O’Sullivan, D., Browse, J., Pringle, K. J., Ardon-  
 1114 Dryer, K., Bertram, A. K., Burrows, S. M., Ceburnis, D., Demott, P. J., Mason, R. H., O’Dowd, C. D.,  
 1115 Rinaldi, M. and Carslaw, K. S.: Contribution of feldspar and marine organic aerosols to global ice  
 1116 nucleating particle concentrations, *Atmos. Chem. Phys.*, 17(5), 3637–3658, doi:10.5194/acp-17-3637-  
 1117 2017, 2017.
- 1118 Vergara-Temprado, J., Miltenberger, A. K., Furtado, K., Grosvenor, D. P., Shipway, B. J., Hill, A. A.,  
 1119 Wilkinson, J. M., Field, P. R., Murray, B. J. and Carslaw, K. S.: Strong control of Southern Ocean cloud  
 1120 reflectivity by ice-nucleating particles, *Proc. Natl. Acad. Sci.*, 115(11), 2687 LP – 2692,  
 1121 doi:10.1073/pnas.1721627115, 2018.
- 1122 Wang, N., Edtbauer, A., Stönnner, C., Pozzer, A., Bourtsoukidis, E., Ernle, L., Dienhart, D., Hottmann, B.,  
 1123 Fischer, H., Schuladen, J., Crowley, J. N., Paris, J.-D., Lelieveld, J. and Williams, J.: Measurements of  
 1124 carbonyl compounds around the Arabian Peninsula: overview and model comparison, *Atmos. Chem.*  
 1125 *Phys.*, 20(18), 10807–10829, doi:10.5194/acp-20-10807-2020, 2020.
- 1126 Wang, X., Deane, G. B., Moore, K. A., Ryder, O. S., Stokes, M. D., Beall, C. M., Collins, D. B.,  
 1127 Santander, M. V., Burrows, S. M., Sultana, C. M. and Prather, K. A.: The role of jet and film drops in  
 1128 controlling the mixing state of submicron sea spray aerosol particles, *Proc. Natl. Acad. Sci.*, 114(27),  
 1129 6978–6983, doi:10.1073/pnas.1702420114, 2017.
- 1130 Welti, A., Lüönd, F., Kanji, Z. A., Stetzer, O. and Lohmann, U.: Time dependence of immersion freezing:  
 1131 an experimental study on size selected kaolinite particles, *Atmos. Chem. Phys.*, 12(20), 9893–9907,  
 1132 doi:10.5194/acp-12-9893-2012, 2012.
- 1133 Wex, H., DeMott, P. J., Tobo, Y., Hartmann, S., Rösch, M., Clauss, T., Tomsche, L., Niedermeier, D. and  
 1134 Stratmann, F.: Kaolinite particles as ice nuclei: learning from the use of different kaolinite samples and  
 1135 different coatings, *Atmos. Chem. Phys.*, 14(11), 5529–5546, doi:10.5194/acp-14-5529-2014, 2014.
- 1136 Whale, T. F., Murray, B. J., O’Sullivan, D., Wilson, T. W., Umo, N. S., Baustian, K. J., Atkinson, J. D.,  
 1137 Workneh, D. A. and Morris, G. J.: A technique for quantifying heterogeneous ice nucleation in microlitre  
 1138 supercooled water droplets, *Atmos. Meas. Tech.*, 8(6), 2437–2447, doi:10.5194/amt-8-2437-2015, 2015.
- 1139 Wilson, T. W., Ladino, L. a., Alpert, P. a., Breckels, M. N., Brooks, I. M., Browse, J., Burrows, S. M.,  
 1140 Carslaw, K. S., Huffman, J. A., Judd, C., Kilthau, W. P., Mason, R. H., McFiggans, G., Miller, L. a.,  
 1141 Nájera, J. J., Polishchuk, E., Rae, S., Schiller, C. L., Si, M., Temprado, J. V., Whale, T. F., Wong, J. P. S.,  
 1142 Wurl, O., Yakobi-Hancock, J. D., Abbatt, J. P. D., Aller, J. Y., Bertram, A. K., Knopf, D. a. and Murray,



- 1143 B. J.: A marine biogenic source of atmospheric ice-nucleating particles, *Nature*, 525(7568), 234–238,  
 1144 doi:10.1038/nature14986, 2015.
- 1145 Wu, W.-S., Purser, R. J. and Parrish, D. F.: Three-Dimensional Variational Analysis with Spatially  
 1146 Inhomogeneous Covariances, *Mon. Weather Rev.*, 130(12), 2905–2916, doi:10.1175/1520-  
 1147 0493(2002)130<2905:TDVAWS>2.0.CO;2, 2002.
- 1148 Yadav, S., Venezia, R. E., Paerl, R. W. and Petters, M. D.: Characterization of Ice-Nucleating Particles  
 1149 Over Northern India, *J. Geophys. Res. Atmos.*, 124(19), 10467–10482,  
 1150 doi:https://doi.org/10.1029/2019JD030702, 2019.
- 1151 Yahya, R. Z., Arrieta, J. M., Cusack, M. and Duarte, C. M.: Airborne Prokaryote and Virus Abundance  
 1152 Over the Red Sea, *Front. Microbiol.*, 10, 1112, doi:10.3389/fmicb.2019.01112, 2019.
- 1153 Yang, J., Wang, Z., Heymsfield, A. J., DeMott, P. J., Twohy, C. H., Suski, K. J. and Toohey, D. W.: High  
 1154 ice concentration observed in tropical maritime stratiform mixed-phase clouds with top temperatures  
 1155 warmer than  $-8^{\circ}\text{C}$ , *Atmos. Res.*, 233, 104719, doi:https://doi.org/10.1016/j.atmosres.2019.104719, 2020.
- 1156 Yost, J. L. and Hartemink, A. E.: Chapter Four - Soil organic carbon in sandy soils: A review, vol. 158,  
 1157 edited by D. L. Sparks, pp. 217–310, Academic Press., 2019.
- 1158 Yu, Y., Kalashnikova, O. V., Garay, M. J., Lee, H. and Notaro, M.: Identification and Characterization of  
 1159 Dust Source Regions Across North Africa and the Middle East Using MISR Satellite Observations,  
 1160 *Geophys. Res. Lett.*, 45(13), 6690–6701, doi:https://doi.org/10.1029/2018GL078324, 2018.
- 1161 Zolles, T., Burkart, J., Häusler, T., Pummer, B., Hitznerberger, R. and Grothe, H.: Identification of Ice  
 1162 Nucleation Active Sites on Feldspar Dust Particles, *J. Phys. Chem. A*, 119(11), 2692–2700,  
 1163 doi:10.1021/jp509839x, 2015.
- 1164